ACS OMEGA

http://pubs.acs.org/journal/acsodf

Article

Thermal Response of Biocarbon-Filled Hemp Fiber-Reinforced Bioepoxy Composites

Raj Kumar Dahal, Bishnu Acharya,* and Animesh Dutta*

Cite This: *ACS Omega* 2023, 8, 15422−15440

Read Online

ACCESS | Metrics & More | Article Recommendations | Supporting Information

ABSTRACT: We investigated the thermal conductivity of materials based on pyrolysis temperature, filler loading, filler size, and type of biomass feedstock. Hemp stalk and switchgrass were pyrolyzed at 450, 550, and 650 °C and crushed into 50, 75, and 100 μm particle sizes. Biocarbon fillers (10, 15, and 20 wt %) were added to the bioepoxy polymer matrix. The study showed increased filler loading and particle size increased thermal conductivity—the biocomposite samples with 20 wt % filler loading of 100 μm particle size of the biocarbon obtained at 650 °C showed the maximum thermal conductivity in both hemp biocarbon-filled composites (0.59 $W{\cdot}m^{-1}{\cdot}K^{-1}$) and switchgrass-filled composites (0.58 $W{\cdot}m^{-1}{\cdot}K^{-1}$) with the highest flame time. Biocarbon in biofiber-reinforced polymer composites can improve thermal conductivity and extend the flame time. These findings significantly contribute to developing hemp-based bioepoxy composite materials for thermal applications in various fields. These include insulating materials for buildings and thermal management systems, energy-efficient applications, and help in material selection and product design with a positive environmental impact.

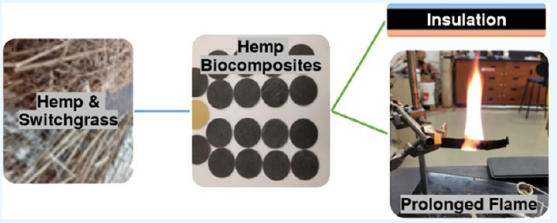

1. INTRODUCTION

The impact on the environment due to the continuous use of fossil-based materials has strongly suggested that future materials should be biobased or at least incorporate biomass in the composites so that fossil fuel use is reduced significantly. Composite materials offer a more comprehensive range of mechanical, electrical, thermal, distinctive physical, chemical, and many other unique properties that the composite's constituent material cannot offer. The urgency to find alternative, environmentally friendly, and sustainable materials with noncompromising mechanical and thermal properties has resulted in numerous research on natural fiber-reinforced polymer composites. Naturally derived fibers such as flax, hemp, jute, sisal, *Hibiscus sabdariffa*, Pinus, jute, pineapple leaf fiber, and oil palm fiber have been practiced since ancient times. Currently, these natural fiber-reinforced polymer composites are being used in various furniture items, instrument panels, internal engine parts, interior and exterior of vehicles, and oil/air filters, and the usage is advancing to more structurally demanding components.[1] Their application in the materials for their unique resultant composite properties is an intriguing factor to consider as a reinforcing and filler element in thermoplastic and thermosetting plastics polymer composites. The resulting composite will have better mechanical properties and durability. Among the many advantages that natural fiber-reinforced polymer composites possess; the lightweight, low density, high specific strength and stiffness, resistance to corrosion, ease of processing, ease of availability, environment-friendly production and disposal, and low cost with competitive strength are some of the significant factors.[1−6] Thermal stability is another vital aspect of a composite material.

The study of the thermal conductivity of biochar-filled bioepoxy hemp fiber composite can provide valuable insights into the material's thermal properties with potential practical implications in various fields, including insulating materials for buildings and thermal management systems for the devices, energy-efficient applications, material selection, and product design with positive impact to the environment.[7,8] The thermal conductivity of a material affects its heat transfer behavior. Its study in biocarbon-bioepoxy-hemp fiber composites can improve the understanding of the insulating efficiency of the material against heat transfer. This understanding is vital in energy-efficient building design and industrial applications. The thermal conductivity of the material enables the engineers to select materials for specific applications; for instance, a thermally highly conductive material is required in devices generating heat to prevent their overheating. This information is helpful for a designer to design products based on efficiency, durability, and effectiveness. Biocarbon fillers obtained from agricultural byproducts are a sustainable material for composite

Received: February 2, 2023
Accepted: April 11, 2023
Published: April 20, 2023

https://doi.org/10.1021/acsomega.3c00700
ACS Omega 2023, 8, 15422−15440

Table 1. Composite Samples and Their Compositions

composites	biocarbon	reinforcement	pyrolysis temperature (°C)	particle size (μ)	filler loading (wt %)
H45-50-10	hemp	hemp	450	50	10
H45-50-20	hemp	hemp	450	50	20
H45-100-10	hemp	hemp	450	100	10
H45-100-20	hemp	hemp	450	100	20
H55-75	hemp	hemp	550	75	15
H65-50-10	hemp	hemp	650	50	10
H65-50-20	hemp	hemp	650	50	20
H65-100-10	hemp	hemp	650	100	10
H65-100-20	hemp	hemp	650	100	20
S45-50-10	switchgrass	hemp	450	50	10
S45-50-20	switchgrass	hemp	450	50	20
S45-100-10	switchgrass	hemp	450	100	10
S45-100-20	switchgrass	hemp	450	100	20
S55-75	switchgrass	hemp	550	75	15
S65-50-10	switchgrass	hemp	650	50	10
S65-50-20	switchgrass	hemp	650	50	20
S65-100-10	switchgrass	hemp	650	100	10
S65-100-20	switchgrass	hemp	650	100	20
HeR	none	hemp	none	none	none
HaR	none	none	none	none	none

preparation. Its usage in material applications leads to sustainable materials with environmental benefits.

The temperature, material's chemical composition, and microstructure[9] are the primary factors influencing its thermal conductivity,[10] and it defines thermal stability, resistance, and tolerance.[11] As a composite contains materials that act as thermal resistances in series, the effective thermal conductivity of composite material is the resultant thermal conductivity of the material contributed by the fiber, resin, and any additives present in the material. Aside from the ingredients of composite material, the constituent fillers' particle size can also change the thermal behavior of the resulting material. The heat transfer through a material subjected to a temperature difference is affected by its chemical composition, the subjected temperature difference, the material's dimensions (cross-sectional area and thickness), and other factors such as the moisture content, carbon content, and morphological character, including the surface finish and attached fins and radiators. For instance, the thermal conductivity due to oxides in ceramics only followed the $1/T$ relationship in a limited temperature range above the Debye temperature.[12] In another study, it was observed that there was a reduction in thermal conductivity when charcoal was used compared to 100% Portland cement.

On the contrary, the effective thermal conductivity increased with the grain size of the sand particles in the polyethylene matrix.[13] In addition, the particle loading and the size reduced the composite material's thermal conductivity.[14] Wood concentration in polyethylene decreased the material's thermal conductivity.[15] Hemp fiber is a naturally herb-derived thread with excellent strength, durability, and natural protection against pests. This vigorous fiber-generating plant has strengthened the structure since the beginning of construction. Currently, hemp plays a significant role as an insulating material in buildings.[16,17] Hemp contributes to thermally insulating and acoustic properties compared with conventional insulations due to its better moisture resistance and capillary water drainage properties. The thermal conductivity of hemp fiber is reported in the range of 0.038 to 0.04 $W{\cdot}m^{-1}{\cdot}K^{-1}$, which is closer to conventional insulation.[16] Hemp fiber decreased the thermal conductivity (K) of the virgin acrylic polymer matrix because of its low value of K. A composite from hemp and polypropylene showed K values ranging from 0.028 up to 0.04 $W{\cdot}m^{-1}{\cdot}K^{-1}$).[18] The thermal resistance of hemp and polybutylene terephthalate co-glutarate composite significantly improved by adding sepiolite, carbon black, and carbon nanotube fillers.[19] Polyurethane-hemp fibers composite presented excellent insulating properties compared to the traditional insulation materials (glass wool, mineral wool).[20] In addition, the hemp fiber content was more responsible for the increased thermal conductivity, indicating that the hemp fiber offers higher thermal conductivity than the polyurethane matrix in the composite.[20] The pore size and the gas trapped in between were explained as the reason for the hemp fibers' remarkable thermal insulating behavior. Even though hemp fiber has found many practical thermal, structural, and aesthetic applications, the hemp hurd (which is approx. 60−80 wt % of core (hemp hurd))[21,22] can find its application in materials to improve their thermal properties when added to the polymer matrix as biocarbon fillers. When combined with a suitable matrix and filler, hemp can produce a sustainable material with desired thermal properties.

Biocarbon can be added to a polymer composite as a filler to improve mechanical strength, electrical conductivity, and thermal stability. The addition of biocarbon may enhance the thermal conductivity of the composite along with improved mechanical properties and reduced weight of the composite material in the case of hemp fiber-reinforced bioepoxy polymer composite. It is worth noting that the specific purpose, for instance, the composite material used in a thermal management application, determines the objective to either increase or decrease the thermal conducting property of the material, and the addition of biocarbon may be specifically targeted at improving this property. In this work, the biocarbon increases the thermal conductivity of the composites suppressed by the hemp-fiber reinforcement.

Although the natural fibers as reinforcement in polymer composites and using biocarbon as a filler material have been

https://doi.org/10.1021/acsomega.3c00700
ACS Omega 2023, 8, 15422−15440

explored, the specific combination of biocarbon-filled hemp fiber-reinforced bioepoxy composites has not been extensively studied. The study fills the research gap in the thermal properties of hemp-based composite materials. This study presents the unexplored area of hemp-reinforced bioepoxy composite filled with biocarbon from hemp and switchgrass. The resulting material's thermal properties will substantially impact the field of composite materials.

2. MATERIALS AND METHOD

2.1. Biocarbon Production. Hemp stalk was obtained from Utopia Hemp company, Ontario, Canada, and switchgrass was obtained from OBPC Farmers, Ontario, Canada. We prepared biocarbon through in-house pyrolysis of the hemp stalk and switchgrass feedstock. Hemp stalk and switchgrass were ground and sieved to 200 μm. Biocarbon was obtained by pyrolyzing the hemp and switchgrass feedstock at three different temperatures (450, 550, and 650 °C) in a nitrogen environment. The nitrogen flow was set to 0.75 L/min, the heating rate was kept at 10 °C/min, and the residence time was 30 min. The biocarbon was left to cool under nitrogen conditions inside the reactor.

2.2. Biocomposite Preparation. Hemp fabric was obtained from Effort Industries Inc., Ontario, Canada. Ecopoxy Biopoxy 36 resin with hardener was purchased from Kitchener Fiberglass, Ontario, Canada. The obtained biocarbon was crushed and sieved into particle sizes below 50 μm, below 75 μm, and 100 μm. Resin and hardener were taken in the ratio of 4:1 by volume. Each hemp-fiber reinforced composite sample used six layers of rectangular hemp fabric (13 cm × 26 cm) with a total weight of 46.6 (± 1.22) g. The biocarbon filler was added to the resin at 10, 15, and 20% by resin weight, and the mixture was stirred for 2 min. A hand-layup technique was implemented to prepare the composite samples, and they were left to cure under a vacuum for 24 h. Table 1 shows a list of composite samples based on the Design Expert software for the full-factorial design of experiments.

2.3. Proximate Analysis. The proximate analysis of the raw samples (hemp stalk and switchgrass) and their biochar samples at various temperatures were performed as per the ASTM standard. The ASTM D3173 was adhered to calculate the moisture in the samples. D3175-20 was followed to analyze the samples' volatile matter, and ASTM E1755-01(2020) adhered to find the ash in the samples. The fixed carbon was calculated from the difference.

2.4. Ultimate Analysis. A Flash 2000 Organic Elemental Analyzer (CHNS-O analyzer) performed the samples' ultimate analysis. The instrument determined carbon, oxygen, nitrogen, and sulfur. Oxygen content was determined from the difference by subtracting the C, H, N, S, and ash content from the total.

2.5. TGA Analysis. The TGA was performed on a TGA: SDT-Q600 (TA Instruments-Waters LLC, USA) instrument. The biocarbon samples were heated to 650 °C as there was negligible weight change after 650 to 1000 °C. The heating rate was kept at 10 °C/min, and the nitrogen flow was maintained at 50 mL/min. For each test, 5−6 mg samples were taken. The tests were repeated for accuracy purposes. The glass transition temperature and the melting point were determined.

2.6. Differential Scanning Calorimetry (DSC). DSC was implemented to study the curing of the thermosets to determine the cross-linking progress during the heating cycles.[23] Differential scanning calorimetry was performed in each sample. The heating rate was again kept at 10 °C/min, nitrogen flow was maintained at 50 mL/min, and the samples were heated to 180 °C. DSC measurements were performed on an SDT-Q600 (TA Instruments-Waters LLC, USA) instrument. Samples (between 5 and 6 mg) were taken in standard alumina pans. All samples were subjected to the following process: (i) heating scan from 25 to 180 °C, hold at 180 °C for 3 min; (ii) cooling scan from 180 to 20 °C; hold at 20 °C for 40 min; (iii) second heating scan from 20 to 180 °C. The heating and cooling rates were set at 10 °C/min.[24]

2.7. Thermal Conductivity. Thermal conductivity was measured by applying the principle demonstrated in Figure 1.

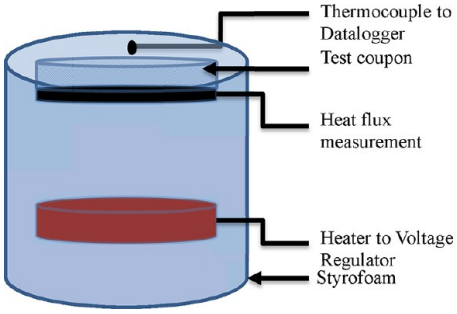

Figure 1. Schematic diagram of thermal conductivity measurement.

The test specimen was heated by a 10 W^2/in-heater. The heater's bottom was insulated with polystyrene foam as insulation, and the heat flux was measured at the bottom side of the sample. A variable autotransformer (3PN1010B, Staco Energy Products Co, USA) supplied a controlled voltage to the heater. The top surface temperatures of the samples were sensed with a T-type thermocouple and recorded with the help of a datalogger (cDAQ-9171, Hungary). The heat supplied to one end of the sample was recorded as provided by the fluxmeter. The resulting temperature due to conducted heat on the upper surface of the samples was left to reach the isothermal state, and the final temperature was recorded. The temperatures at the upper surface of the sample were sensed with multiple T-type thermocouples and registered with the help of a datalogger (cDAQ-9171, Hungary). The thermal conductivity (K) was measured as follows:

$$K = \frac{q \cdot t}{\mathrm{d}T}$$

where q is the heat flux, t is the thickness of the sample, and dT is the temperature difference across the sample.

A schematic diagram is presented in Figure 1 below to demonstrate the measurement of the thermal conductivity of the composite samples.

2.8. Flame Test. The flame test was performed under an ASTM D635. A 20 ± 2 mm high blue flame was applied at an angle of 45 ± 2° to one end of the horizontally clamped samples so that the test flame impinges on the free end of the test specimen to a depth of approximately 6 mm, starting the timing device simultaneously. The flame was applied for 30 ± 1 s or until the flame front reached the 25 mm mark. Then, the flame travel time from the 25 mm reference mark to the 100 mm reference mark was recorded as t (s). The burned length (L) in mm was measured as the distance between the 25 mm reference mark and the flame front stop position.

2.9. SEM Analysis. The surface morphology of the composites was studied under the FEI Quanta 250 field emission scanning electron microscope (FE-SEM) by generat-

https://doi.org/10.1021/acsomega.3c00700
ACS Omega 2023, 8, 15422−15440

Table 2. Chemical and Proximate Analyses of the Biomasses and Their Biocarbon Products at 450, 550, and 650 °C[a]

	H	H450	H550	H650	S	S450	S550	S650
moisture	7.26 (±0.03)	3.17 (±0.01)	1.56 (±0.11)	1.59 (±0.09)	5.47 (±0.09)	1.19 (±0.10)	1.28 (±0.20)	0.25 (±0.26)
VM (wet)	73.34 (±0.97)	23.30 (±0.34)	18.94 (±0.57)	14.86 (±0.26)	82.71 (±0.48)	21.52 (±0.02)	11.71 (±0.67)	10.17 (±0.24)
ash (dry)	3.56 (±0.20)	8.29 (±0.36)	13.05 (±0.24)	13.88 (±0.19)	1.35 (±0.14)	10.86 (±0.26)	12.47 (±0.03)	8.22 (±0.27)
FC (dry)	8.53	62.08	66.45	68.08	5.01	65.23	73.26	81.11
N	0.35 (±0.05)	0.82 (±0.00)	0.85 (±0.05)	0.71 (±0.08)	1.41 (±0.08)	1.40 (±0.14	1.10 (±0.07)	0.98 (±0.03)
C	45.34 (±0.25)	71.06 (±0.26)	73.88 (±0.52)	73.54 (±0.21)	43.35 (±0.27)	73.20 (±0.02)	80.54 (±0.25)	82.03 (±0.39)
H	5.91 (±0.15)	2.90 (±0.03)	2.16 (±0.01)	1.67 (±0.07)	5.93 (±0.09)	2.89 (±0.18)	2.35 (±0.05)	1.62 (±0.01)
S	0 (±0.00)	0.03 (±0.04)	0 (±0.00)	0.05 (±0.01)	0.09 (±0.00)	0 (±0.00)	0 (±0.00)	0 (±0.00)
O	47.05	14.32	10.64	15.81	45.66	14.22	2.95	1.48

[a]VM = volatile matter, FC = fixed carbon, H = hemp stalk, S = switchgrass, H450 = biocarbon from hemp at 450 °C, H550 = H biocarbon from hemp at 550 °C, H650 = biocarbon from hemp at 650 °C, S450 = biocarbon from switchgrass at 450 °C, S550 = biocarbon from switchgrass at 550 °C, S650 = biocarbon from switchgrass at 650 °C.

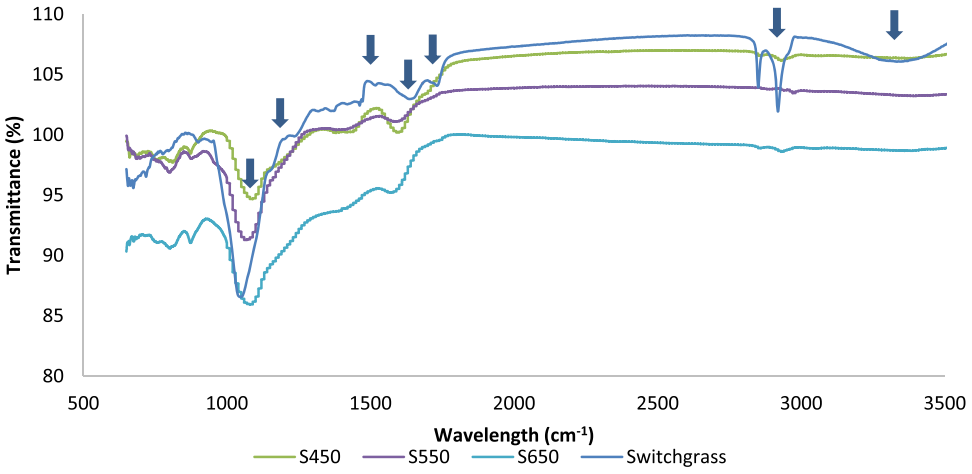

Figure 2. Raw switchgrass's FTIR curves and its various biocarbon samples.

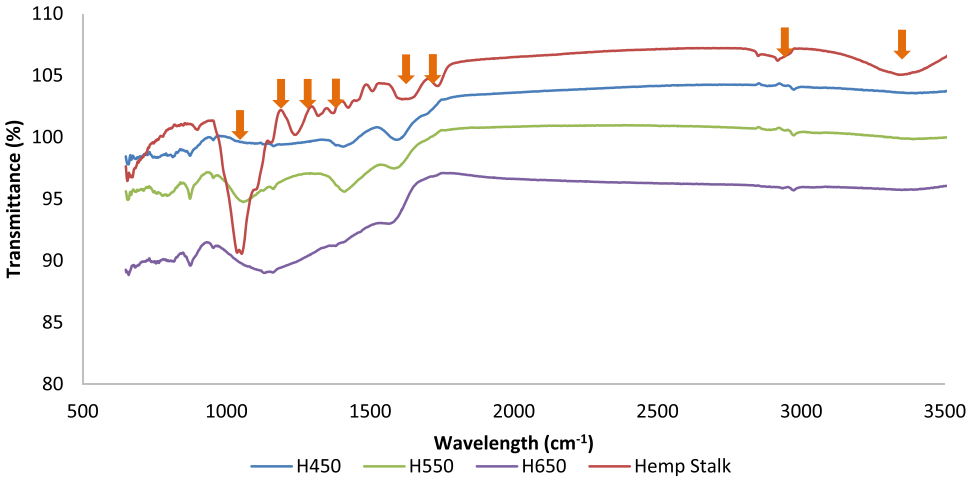

Figure 3. FTIR curves of the raw hemp stalk and its various biocarbon samples.

ing the magnified cross-sectional views on the tested tensile samples. The accelerating voltage was set to 20 kV, and a working distance of 10 mm was maintained. The instrument was set to 4.19×10^{-6} bar vacuum pressure. The samples obtained from the tensile tests were fractured in normal room conditions by shearing with a bolt cutter. Before microscopic imaging, each sample was sputter-coated under Helium in a Desk V Denton Vacuum instrument.

2.10. Data Analysis. The data from the thermal tests were statistically analyzed with a confidence level of 95% for all the composites (p-value 0.05). The average values with standard deviations were reported. One-way analysis of variance (ANOVA) was performed using Design Expert statistical software, and optimization was performed.

3. RESULTS AND DISCUSSION

3.1. Biocarbon Physiochemical Properties. Table 2 below summarizes the physiochemical properties of the raw hemp and switchgrass feedstock. Table 2 also includes the

https://doi.org/10.1021/acsomega.3c00700
ACS Omega 2023, 8, 15422−15440

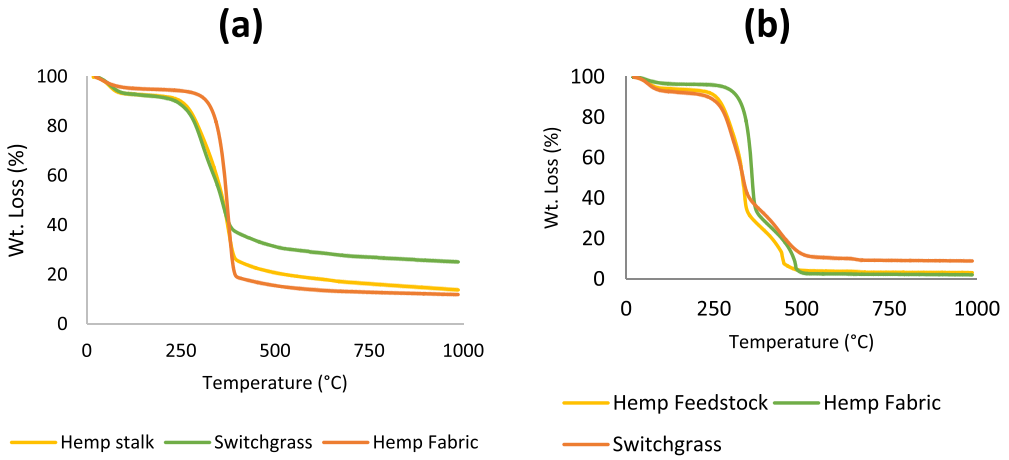

Figure 4. Thermal degradation of hemp and switchgrass feedstock (a) under nitrogen and (b) in air.

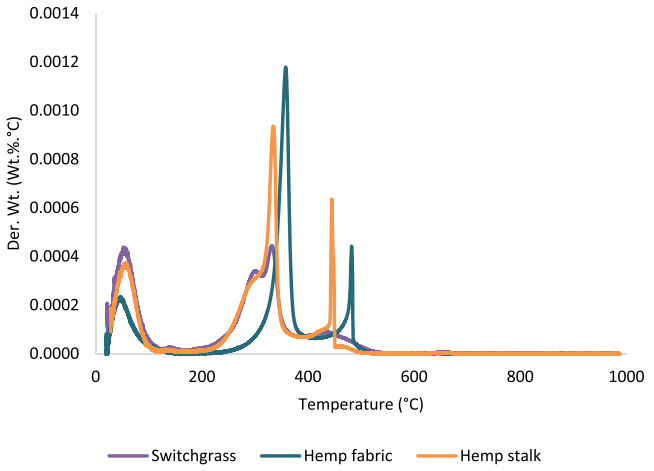

Figure 5. Differential thermogravimetric (DTG) curve of hemp and switchgrass feedstock.

Table 3. Glass Transition Temperature of the Hemp Composites at Two Heating Cycles during the DSC Analysis

			hemp biocarbon composites		switchgrass biocarbon composites	
factor 1	factor 2	factor 3	first cycle	second cycle	first cycle	second cycle
A: pyrolysis temperature	B: particle size	C: filler loading	T_g	T_g	T_g	T_g
650	100	10	69.22	76.49	70.43	76.95
650	100	20	70.31	76.05	70.55	77.09
650	50	20	70.85	76.79	67.94	74.84
650	50	10	69.46	75.88	71	76.28
450	100	20	70.2	75.79	69.67	75.24
550	75	15	70.04	76.57	69.02	77.52
450	50	10	66.96	75.13	69.52	77.2
450	100	10	69.87	76.62	70.05	76.57
450	50	20	70.6	75.87	71.5	76.79

properties of their biocarbon samples obtained at three different temperatures (450, 550, and 650 °C).

3.2. Fourier Transform Infrared (FTIR) Analysis. *3.2.1. Discussion on FTIR of Raw Samples.* The purpose of the FTIR is to characterize biomass[25] and to see the change in chemical composition, functionalization, and transformations in the biocarbon samples compared to their respective feedstocks. Comparative infrared spectroscopy of the raw samples with their respective biocarbon is shown in Figures 2 and 3 below.

The IR spectra of the raw biomasses and their respective biocarbon are shown in Figures 2 and 3. The absorption at 3360 cm^{-1} in the spectra of the raw feedstock (hemp and switchgrass) shows strong O−H stretching in hemicellulose, cellulose,[26] and lignin.[27] The presence of cellulose, hemicellulose, lignin, largely C−H bonds, and hydroxyl groups have

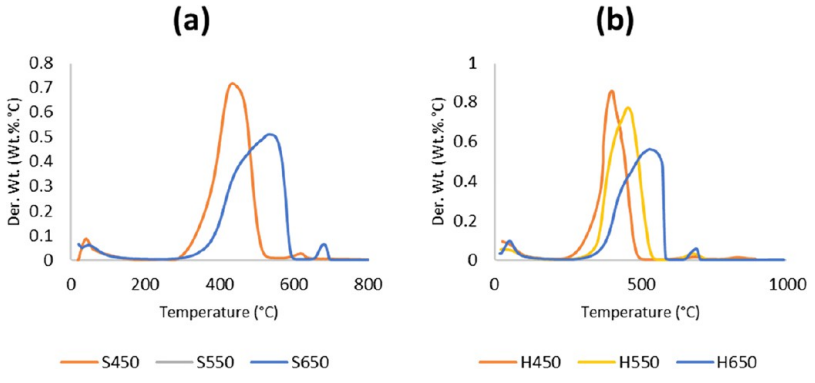

Figure 6. DTG curve of (a) switchgrass biocarbon and (b) hemp biocarbon at 450, 550, and 650 °C.

https://doi.org/10.1021/acsomega.3c00700
ACS Omega 2023, 8, 15422−15440

Table 4. Thermal Conductivity of Biocarbon-Filled Hemp Fiber-Reinforced Polymer Composites

hemp biocarbon composites				switchgrass biocarbon composites			
factor 1 A: pyrolysis temperature	factor 2 B: particle size	factor 3 C: filler loading	thermal conductivity ($W \cdot m^{-1} \cdot K^{-1}$)	factor 1 A: pyrolysis temperature	factor 2 B: particle size	factor 3 C: filler loading	thermal conductivity ($W \cdot m^{-1} \cdot K^{-1}$)
550	75	15	0.489	450	100	20	0.514
650	100	10	0.596	450	50	10	0.391
450	50	10	0.382	650	100	20	0.634
650	100	10	0.523	650	100	10	0.409
650	100	20	0.632	650	50	10	0.361
650	100	20	0.636	450	50	10	0.430
650	50	10	0.391	450	50	20	0.475
450	50	10	0.371	650	100	20	0.612
450	100	20	0.598	450	50	20	0.454
450	50	10	0.462	650	50	10	0.368
450	100	10	0.476	650	50	20	0.392
550	75	15	0.473	650	100	10	0.440
650	50	10	0.388	650	50	20	0.385
650	50	20	0.467	450	50	20	0.450
450	50	10	0.447	650	100	10	0.462
650	100	20	0.496	450	100	10	0.478
450	50	20	0.421	550	75	15	0.441
450	100	20	0.531	450	100	20	0.579
450	100	20	0.482	550	75	15	0.449
450	100	10	0.561	650	50	10	0.362
450	50	20	0.436	650	100	10	0.461
650	50	20	0.442	450	100	10	0.469
650	100	10	0.563				
550	75	15	0.448				
450	100	10	0.429				
650	50	20	0.507				
450	100	10	0.449				
450	50	10	0.331				
650	50	20	0.438				
450	100	10	0.427				
450	50	10	0.417				
450	50	20	0.388				
450	50	20	0.418				
550	75	15	0.461				
450	100	10	0.391				
450	100	10	0.493				

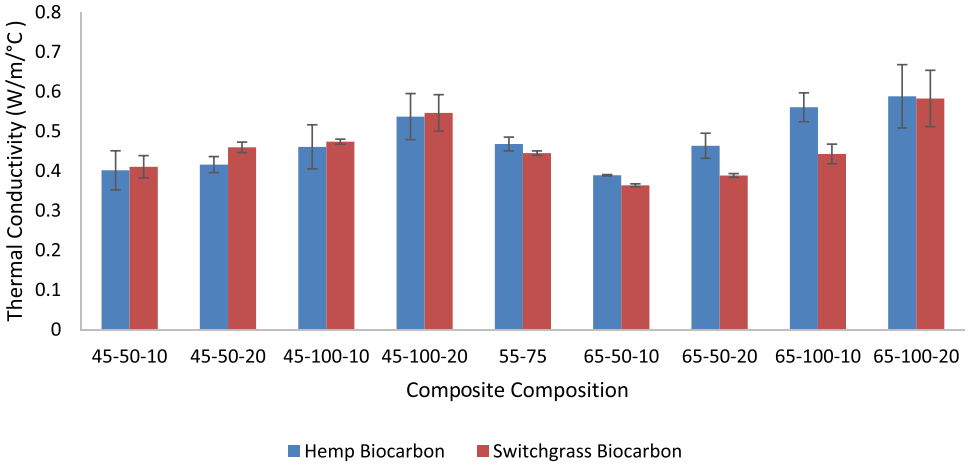

Figure 7. Comparison of thermal conductivity between hemp and switchgrass biocarbon fillers in the hemp fiber-reinforced composite samples.

https://doi.org/10.1021/acsomega.3c00700
ACS Omega 2023, 8, 15422−15440

Table 5. ANOVA Table for the Factorial Model of the Biocarbon-Filled Polymer Composite Samples (Response: Thermal Conductivity, Power Transformed, λ: −0.5 for Hemp Biocarbon-Filled, and −1.5 for Switchgrass Biocarbon-Filled Samples Statistical Models)

	hemp biocarbon-filled samples					switchgrass biocarbon-filled samples				
source hemp	sum of squares	df	mean square	*F*-value	*p*-value	sum of squares	df	mean square	*F*-value	*p*-value
model	0.2786	3	0.0929	18.1	< 0.0001	11.03	6	1.84	39.49	< 0.0001
A-pyrolysis temperature	0.0385	1	0.0385	7.5	0.01	0.7389	1	0.7389	15.88	0.0012
B-filler size	0.1986	1	0.1986	38.71	< 0.0001	6.56	1	6.56	140.94	< 0.0001
C-filler loading	0.0373	1	0.0373	7.27	0.0111	2.69	1	2.69	57.89	< 0.0001
AB						0.8796	1	0.8796	18.9	0.0006
BC						0.2695	1	0.2695	5.79	0.0294
ABC						0.2685	1	0.2685	5.77	0.0297
residual	0.1642	32	0.0051			0.698	15	0.0465		
lack of fit	0.0237	5	0.0047	0.9107	0.4888	0.1148	2	0.0574	1.28	0.3108
pure error	0.1405	27	0.0052			0.5831	13	0.0449		
cor total	0.4428	35				11.72	21			

Table 6. Fit Statistics for the Biocarbon-Filled Polymer Composites

samples	std. dev.	mean	R^2	adjusted R^2	predicted R^2	CV (%)
hemp biocarbon composites	0.0716	1	0.63	0.59	0.53	4.86
switchgrass biocarbon composites	0.2157	3	0.94	0.92	0.86	6.35

caused these considerable absorptions. At 2920 and 2850 cm^{-1}, the absorptions in both feeds were due to the C−H stretching in lignin,[27] cellulose, and hemicellulose.[26] Absorption at 1730 cm^{-1} in switchgrass is due to the stretching of C═O in ketone/aldehyde in hemicellulose,[28] pectin, and waxes.[26]

Absorption in hemp stalk at 1750 cm^{-1} is due to pectic acid and free ester in hemicellulose.[28] The unconjugated C═O stretching[27] and the OH bending of absorbed water[26] in both biomass samples caused the absorption at 1650 cm^{-1}. Aromatic ring vibration and C═O stretching in lignin[28] present in hemp are attributed to the absorption at 1600 cm^{-1}. The absorption at 1520 cm^{-1} is attributed to the C═C aromatic ring vibration in lignin[26,28] in both samples. Absorptions at 1465 cm^{-1} in both feeds are due to the C−H deformation in lignin.[28] The absorption observed in hemp stalk at 1430 cm^{-1} is attributed to the C−H in-plane deformation and O−H in-plane bending in cellulose and lignin.[26,28] The C−H bending in cellulose, hemicellulose, and lignin[28] caused the absorption at 1380 cm^{-1} in both raw feedstocks. The peak seen at 1320 cm^{-1} in the hemp sample is due to the presence of the C−H bond of the syringyl ring in lignin[27] and CH_2 rocking vibration in cellulose.[26]

The peaks observed at 1300−600 cm^{-1} in all samples result from infrared absorbance by low molecular weight carbohydrates, polyols, and monosaccharides; this region is known as the fingerprint region.[29,30] C−C and C−O stretching,[27] aromatic ring vibration in Guaiacyl lignin,[28] and C═O and G ring stretching in lignin[26] caused the absorptions at 1240 cm^{-1} in the raw biomass samples. In switchgrass, the symmetrical stretching of C−O−C[26] and bending of O−H in cellulose and hemicellulose[28] resulted in absorption at 1200 cm^{-1}. Both samples showed absorptions at 1160 cm^{-1} due to the asymmetrical stretching of C−O−C in cellulose and hemicellulose.[26,28] In hemp, the symmetrical stretching of C−O−C in ester groups present in cellulose and hemicellulose[31,32] and in-plane deformation of aromatic C−H in lignin[33] caused absorption at 1110 cm^{-1}. The IR spectra showed absorptions in both samples at 1050 cm^{-1}, attributed to the C−O, C═O, and C−C−O stretching in cellulose, hemicellulose, and lignin[26,28] and symmetrical stretching of C−O−C in aliphatic groups and acid derivatives.[31] Glycosidic linkage in cellulose and hemicellulose caused the absorption in IR spectra in both samples at 930 and 860 cm^{-1}.[28] C−O−C, C−C−O, and C−C−H deformation and stretching in cellulose peaked at 900 cm^{-1} in switchgrass.[26] Absorptions at 850 and 833 cm^{-1} were associated with the out-of-plane bending of aromatic C−H in phenolic compounds[33] and the out-of-plane bending of lignin,[32] respectively. CH_2 rocking bending in waxes present in samples is attributed to the peaks at 720 cm^{-1}.[32] Both samples experienced absorption at 660 cm^{-1} due to the C−OH out-of-plane bending in cellulose.[26]

Table 7. Coefficients of Coded Factors for Biocarbon-Filled Polymer Composites

	hemp biocarbon-filled samples						switchgrass biocarbon-filled samples					
factor	coef. est.	df	std. err.	95% CI low	95% CI high	VIF	coef. est.	df	std. err.	95% CI low	95% CI high	VIF
intercept	1.46	1	0.0123	1.44	1.49		3.3546	1	0.0467	3.2549	3.4542	
A-pyrolysis temperature	−0.0367	1	0.0134	−0.064	−0.0094	1.06	0.1980	1	0.0497	0.0921	0.3039	1.05
B-filler size	−0.0795	1	0.0128	−0.1055	−0.0534	1.02	−0.5915	1	0.0498	−0.6977	−0.4853	1.07
C-filler loading	−0.0356	1	0.0132	−0.0625	−0.0087	1.07	−0.3781	1	0.0497	−0.4840	−0.2722	1.05
AB							−0.2160	1	0.0497	−0.3220	−0.1101	1.05
BC							−0.1196	1	0.0497	−0.2255	−0.0137	1.05
ABC							−0.1197	1	0.0498	−0.2259	−0.0135	1.07

https://doi.org/10.1021/acsomega.3c00700
ACS Omega 2023, 8, 15422−15440

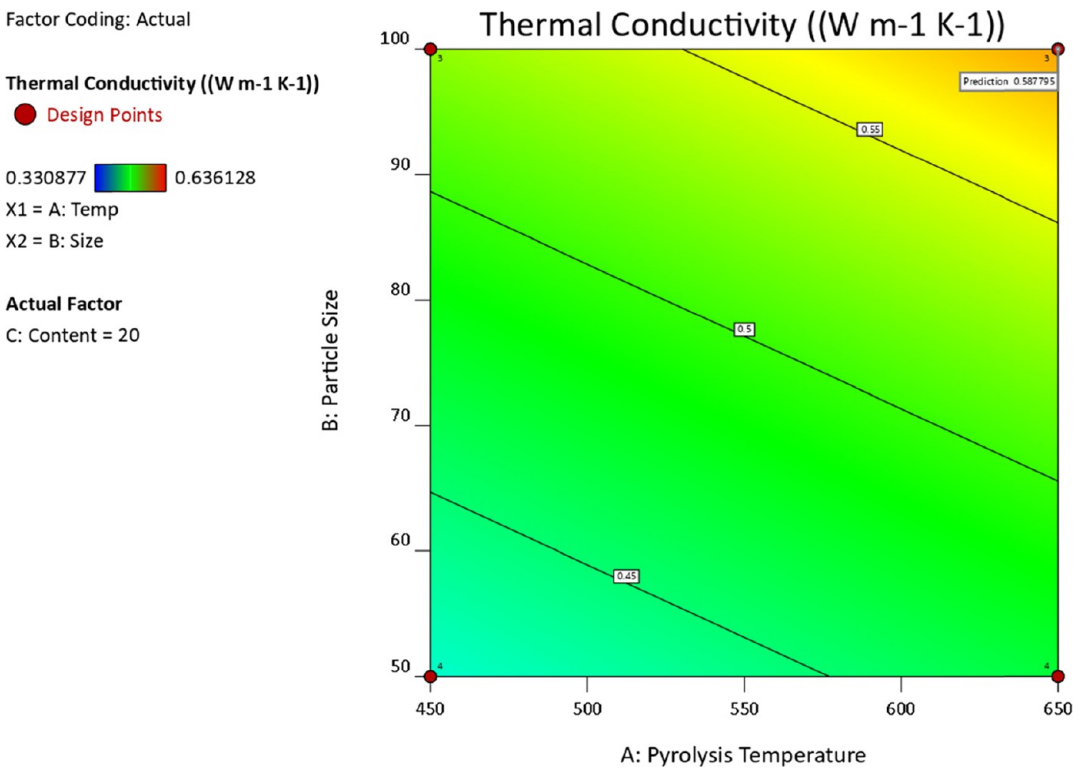

Figure 8. Contour plot of the thermal conductivity of the various hemp biocarbon-filled hemp-reinforced polymer composites.

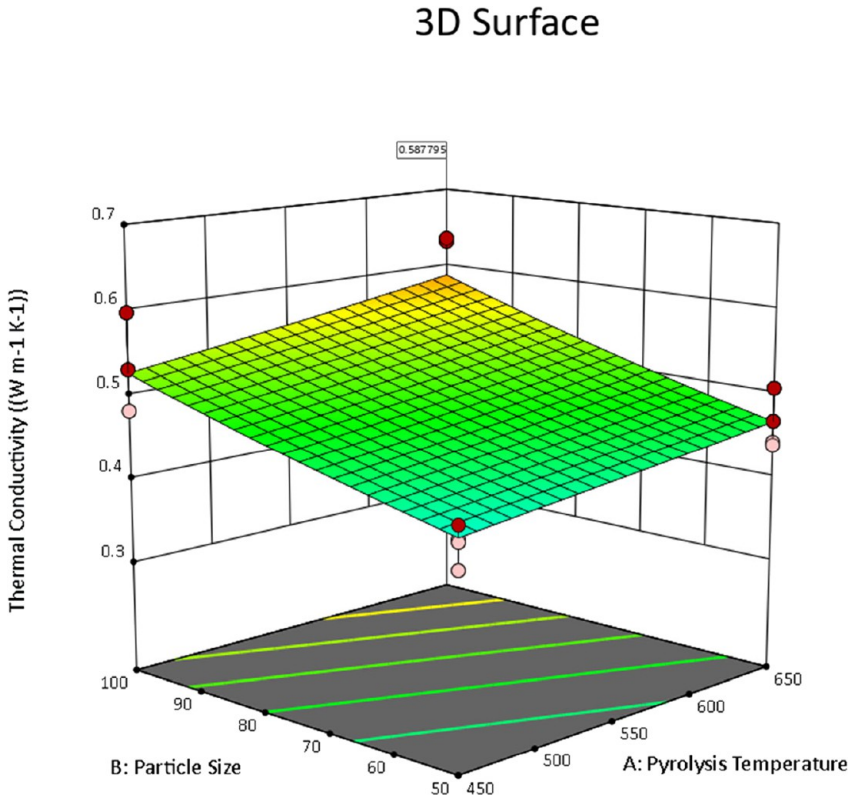

Figure 9. 3D surface response in terms of thermal conductivity of the hemp biocarbon-filled hemp-reinforced polymer composites at the filler loading of 20 wt %.

3.2.2. Discussion on FTIR Spectra of Biocarbon Samples. The elimination of IR absorption at 3360 cm^{-1} in biocarbon samples indicates the elimination of unstable alcoholic, phenolic, and hydroxyl groups at elevated temperatures, which also has been attributed to the accelerated dehydration process in pyrolysis.[34−37,31] The aromatic carbon groups and aliphatic CH_2 groups in lignin were seen to be resistant to the increased pyrolysis temperatures indicated by the presence of a

https://doi.org/10.1021/acsomega.3c00700
ACS Omega 2023, 8, 15422−15440

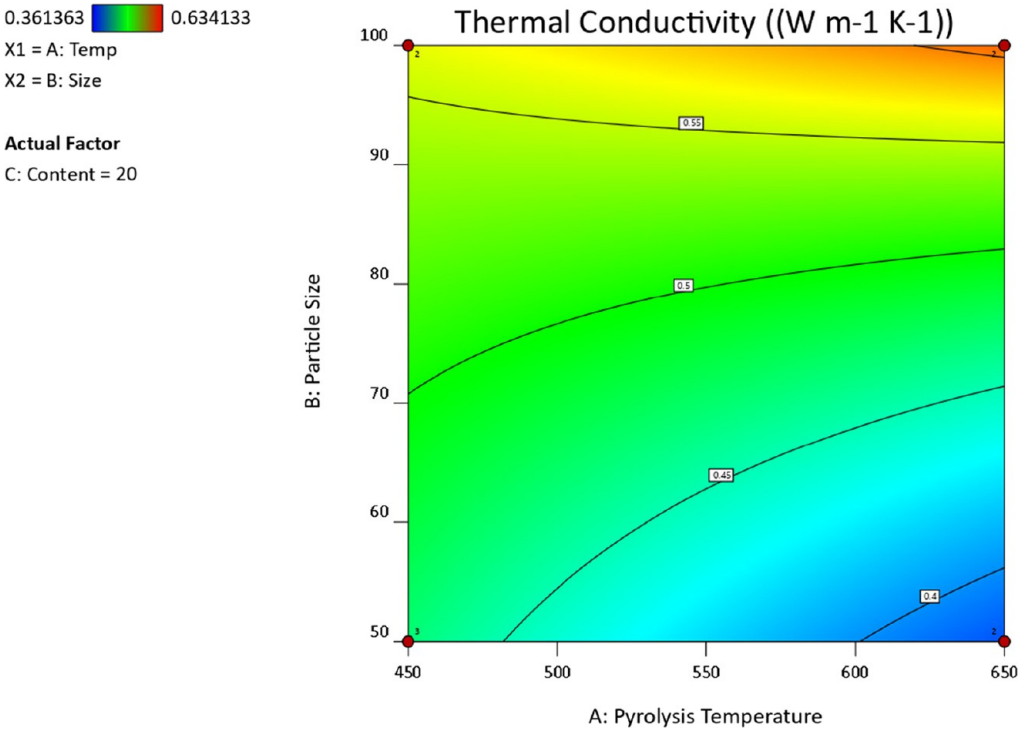

Figure 10. Contour plot of the thermal conductivity of the various switchgrass biocarbon-filled hemp-reinforced polymer composites when the filler loading is 20 wt %.

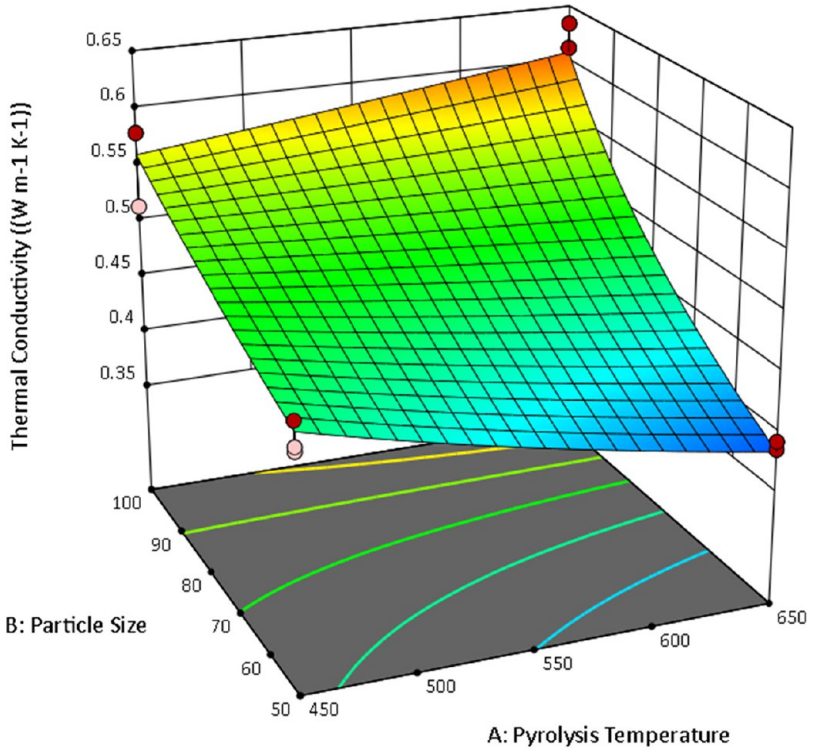

Figure 11. 3D surface response in terms of thermal conductivity of the switchgrass biocarbon-filled hemp-reinforced polymer composites at the filler loading of 20 wt %.

peak in 1400 cm^{-1}.[31] Similarly, the drastic reduction in absorption at 2920 and 2860 cm^{-1} is attributed to the reduction of waxes and aliphatic CH stretching vibration due to the removal of weaker C−H bonds of alkyl groups.[35] Figures 2 and 3 are due to the presence of C═O stretching of methyl ester and carboxylic acid in pectin (containing both esterified and carboxylic acid groups)[38] and waxes, while the hemicellulose, cellulose, and lignin were responsible for the absorption at 2850 cm^{-1}[39] in raw hemp and switchgrass samples. The disappearance of these peaks in biocarbon

https://doi.org/10.1021/acsomega.3c00700
ACS Omega 2023, 8, 15422−15440

Figure 12. Test coupon under the flame test as per the standard.

samples suggests the elimination of waxes, pectin, and hemicellulose in raw samples; the biocarbon is free from those.

Similarly, the preserved aromatic ring, the C═O stretching in lignin,[28] and the presence of polyphenols[40] in the biocarbon samples caused the absorptions at 1600 cm^{-1}. The biocarbon samples also showed the presence of aromatic C−H in lignin[33] associated with the absorption at 1110 cm^{-1}. The reappearing absorptions in biocarbon at 850 cm^{-1} were due to aromatic C−H in phenolic compounds.[33] The absorptions between 800 and 600 cm^{-1} are due to the wagging vibration of the C−H bond in aromatic and heteroaromatic compounds that are visibly preserved in all biocarbon samples compared to their parent biomass samples.[34] The spectra showing the shifting of the baseline toward the left in the biochar samples at higher temperatures are associated with the loss of the functional group and improved graphitization of the biocarbon samples.[41]

3.3. Thermogravimetric Analysis. *3.3.1. TGA of Raw Biomass.* The TGA and DTG results of the hemp fabric, hemp stalk, and switchgrass are shown in Figures 4 and 5 below, respectively.

Hemp stalk mainly contains pectin that binds microfibrils and elementary fibers together. Hemp has an amorphous-structured and low-strength hemicellulose that provides structural tissue support. The hemp plant's cellulose is hydrolysis resistant and bonds hemicellulose with cellulose microfibrils. Moreover, stiff lignin supports plant tissue while transporting food and water. The cellulose, hemicellulose, and pectin are surrounded by lignin.[42] The hemp hurd contains 40−48% cellulose compared to 57−77% cellulose in fibers, 18−24% hemicellulose compared to 9−14% fibers, and 21−24% lignin compared to 5−9% in fibers.[21,22]

Similarly, switchgrass comprises approximately 35% cellulose, 30% hemicellulose, and 9% lignin.[43] Therefore, with similar compounds present in both the feedstock, the thermal degradation of switchgrass is similar to that of the hemp stalk showing thermal breakdown at similar temperatures in the thermogravimetric analysis of biomass feedstock (hemp and switchgrass) shown in Figures 2 and 3. The curves show three distinctive zones of thermal degradation. The drying stage is followed by the devolatilization of the biomass and the combustion of fixed carbon, turning it into ash. The loss of free water and lower volatile matters from the raw material contributed to approx. 6, 7, and 5% mass loss in hemp stalk, switchgrass, and fabric, respectively. The moisture loss and loss of lower volatile compounds continued till approx. 120 °C in all biomass samples. The second decomposition shoulder peak at approx. 200 to 305 °C in hemp stalk and switchgrass was due to the thermal depolymerization of hemicellulose, and pectin occurs.[38] The switchgrass showed the maximum hemicellulose degradation peak at approx. 300 °C. The continued peak from the peak shoulder of hemicellulose till 390 °C mainly shows the thermal decomposition of cellulosic material in the raw switchgrass and hemp stalk samples. The maximum degradation of cellulose in hemp stalk was observed at 335 °C and was close to that of switchgrass at 330 °C. In Figure 3, it is evident that the removal of hemicellulose caused the removal of the shouldering peak from the hemp fabric DTG curve. The offsetting of the cellulosic decomposition peak by approx. 35 °C in hemp fabric (at 358 °C) from the hemp stalk (at 335 °C) demonstrates its improved thermal resilience.

Further, the depolymerization of lignin resulted in a peak above 390 °C in hemp stalk and switchgrass. Max lignin decomposed at 435 °C in switchgrass and 445 °C, indicating thermal resistant heavily cross-linked lignin in hemp stalk compared to the switchgrass. The chemical treatment of hemp fiber to obtain fabric caused thermally more stable lignin hemp fabric indicated by its offset peak ranging from 415 °C to 520 and maxing at 482 °C. The lignin degradation peak shifted by

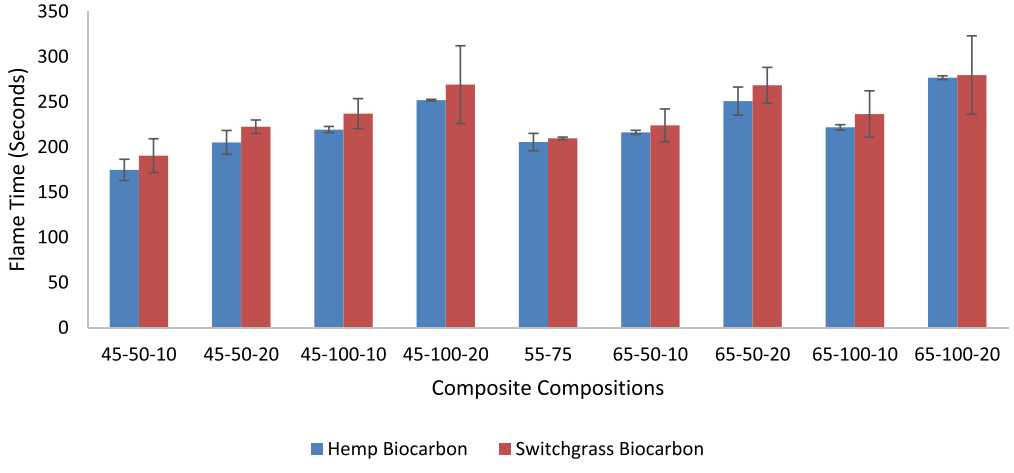

Figure 13. Comparison flame time (s) between hemp and switchgrass biocarbon fillers in the hemp fiber-reinforced composite samples.

https://doi.org/10.1021/acsomega.3c00700
ACS Omega 2023, 8, 15422−15440

Table 8. ANOVA Table for the Hemp Biocarbon and Switchgrass Biocarbon-Filled Hemp-Reinforced Polymer Composites

	hemp biocarbon-filled composites (power transformed, λ = 2.25)					switchgrass biocarbon-filled composites (power transformed, λ = −1.8)				
source	SS ($\times 10^8$)	df	MS ($\times 10^8$)	F-value	p-value	SS ($\times 10^{-10}$)	df	MS ($\times 10^{-11}$)	F-value	p-value
model	584	6	97.3	39.46	<0.0001	25	4	62.4	7.47	0.0014
A-pyrolysis temperature	133	1	133	53.77	<0.0001	4.82	1	48.2	5.76	0.0289
B-particle size	147	1	147	59.53	<0.0001	7.00	1	70.0	8.37	0.0106
C-filler loading	249	1	249	101.04	<0.0001	10.1	1	101	12.03	0.0032
AB	22.8	1	22.8	9.26	0.0112	3.29	1	32.9	3.93	0.0647
AC	16.6	1	16.6	6.73	0.025					
BC	12.3	1	12.3	4.97	0.0475					
curvature	35.7	1	35.7	14.49	0.0029					
residual	27.1	11	2.47			13.4	16	8.36		
lack of fit	2.59	1	2.59	1.06	0.3285	3.21	4	8.02	0.947	0.4704
pure error	24.5	10	2.45			10.2	12	8.47		
cor total	646	18				38.4	20			

Table 9. Fit Statistics for the Statistical Models of the Hemp Biocarbon and Switchgrass Biocarbon-Filled Hemp-Reinforced Polymer Composites

samples	std. dev.	mean	CV (%)	R^2	adjusted R^2	predicted R^2	adeq. precision
hemp biocarbon-filled composites	15700.34	2.03×10^5	7.74	0.9556	0.9314	0.8576	18.9159
switchgrass biocarbon-filled composites	9.14×10^{-6}	0.0001	16.83	0.6512	0.564	0.4168	8.3309

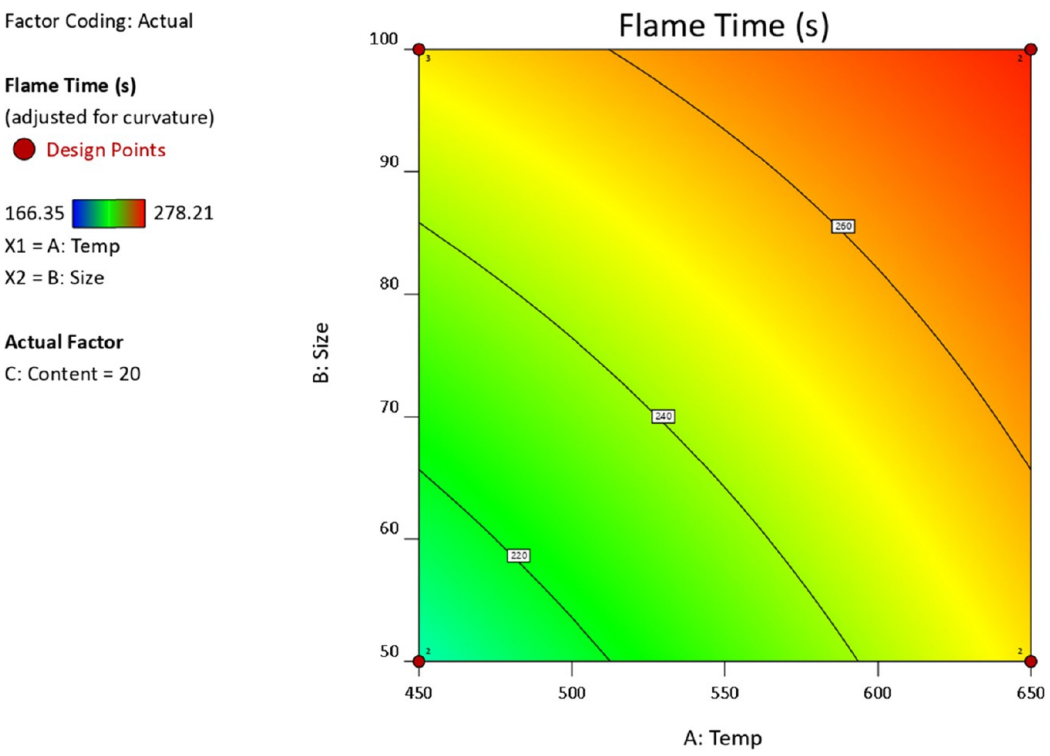

Figure 14. Contour plot of the flame time of the various hemp biocarbon-filled hemp-reinforced polymer composites when filler loading is 20 wt %.

37 °C toward higher temperatures in hemp fabric than the hemp stalk.

The heat-resistance index (HRI) was calculated using the equation HRI = 0.49 (T_5 + 0.6(T_{30} − T_5)), where T_5 and T_{30} are the 5 and 30% thermal degradations of the samples, respectively.[44,45] The HRI of the hemp fabric (HRI = 157) was higher than the hemp stalk by 47%, indicating a thermally stable fabric compared to the raw hemp stalk. The comparison with the switchgrass showed a similar result.

3.3.2. TGA of BIOCARBON Samples. The thermal degradation of various hemp biocarbon and switchgrass biocarbon is presented in Figure 4 below. There were three thermal degradation zones in biocarbon samples similar to that in raw biomass samples. The initial peak was due to the samples' dehydration, followed by the devolatilization of the biocarbon and burning of the residual matter. The biocarbon obtained at different temperatures showed similar degradation zones and patterns. The significant difference is the curve shifting toward the higher temperature for the biocarbon

https://doi.org/10.1021/acsomega.3c00700
ACS Omega 2023, 8, 15422−15440

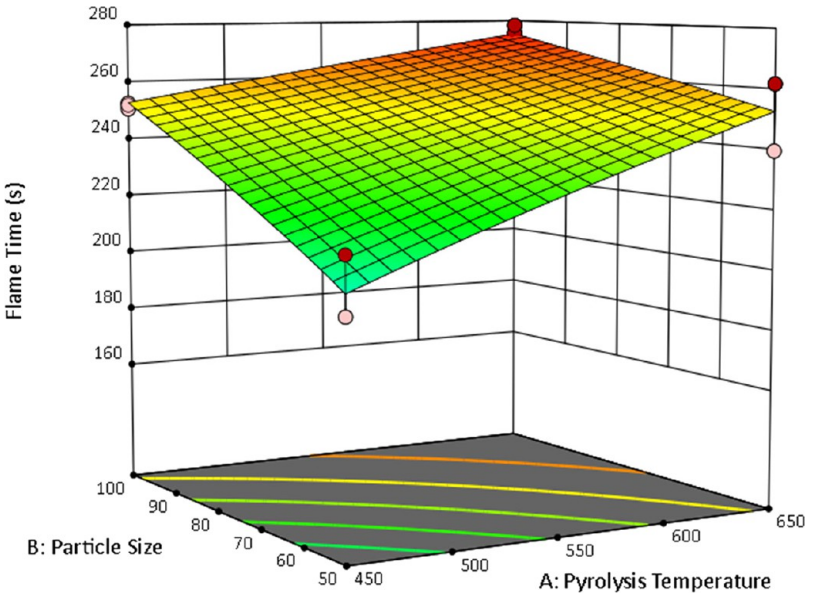

Figure 15. 3D surface response regarding the flame time of the hemp biocarbon-filled hemp-reinforced polymer composites at the filler loading of 20 wt %.

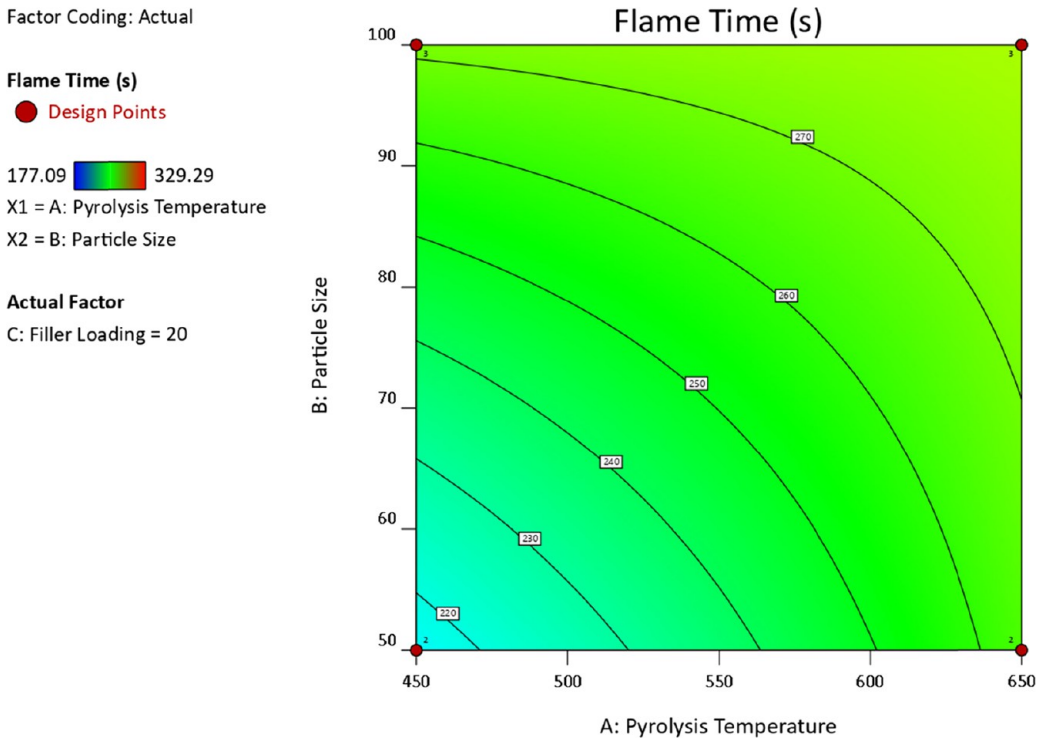

Figure 16. Contour plot of the flame time of the various switchgrass biocarbon-filled hemp-reinforced polymer composites when filler loading is 20 wt %.

obtained at a higher temperature. The significant removal of volatile matters in biochar resulted in stable biocarbon samples in which the devolatilization started at approx. 250 °C and continued until 490 °C reaching the maximum decomposition rate at 398 °C for H450. Char oxidation in the third stage was seen above 640 °C. H550 was thermally more stable than H450 as the volatile started releasing only after 280 °C and stopped at 545 °C. The max degradation was observed at 455 °C. Here, too, the oxidation of the sample took place after 640 °C. Finally, H650 was seen to be the most stable sample against heat. Like in H550, devolatilization started at 280 °C and continued until 580 °C, reaching the maximum degradation rate at 533 °C. The remaining residue oxidized at a temperature above 650 °C. Initial degradation due to moisture removal was seen in a similar temperature range.

In the case of biocarbon obtained from switchgrass, the curve pattern was similar to that of hemp biocarbon as shown in Figure 6. Initial removal of water content till approx. 150 °C was subsequently followed by the peaks representing the release of volatile matter in the biocarbon samples. Here, S450

https://doi.org/10.1021/acsomega.3c00700
ACS Omega 2023, 8, 15422−15440

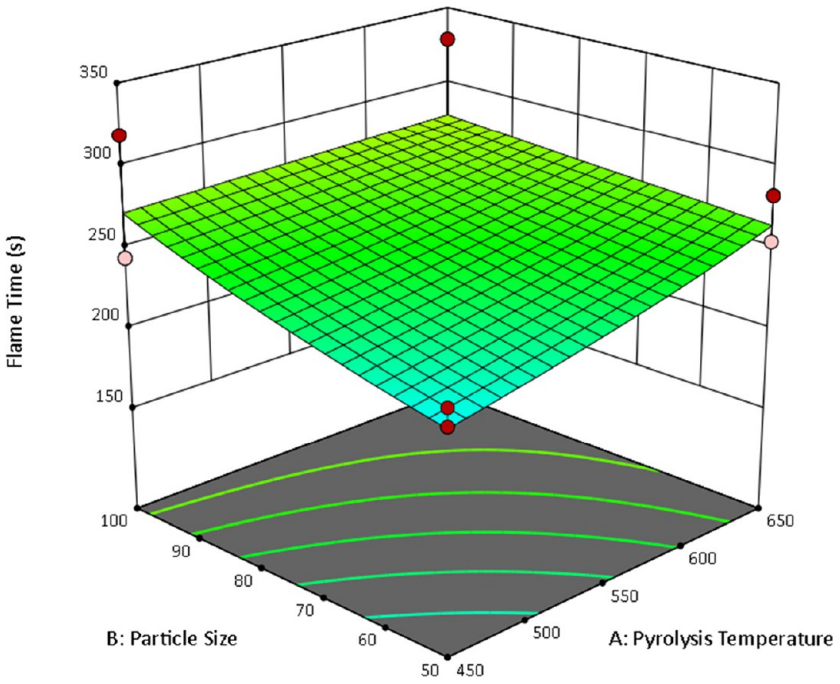

Figure 17. 3D surface response in terms of the flame time of the switchgrass biocarbon-filled hemp-reinforced polymer composites at the filler loading of 20 wt %.

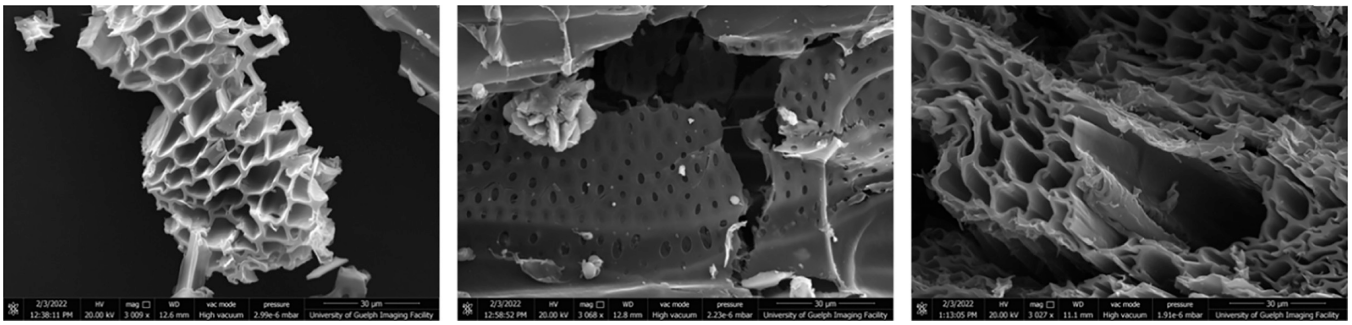

Figure 18. SEM images of hemp biocarbon obtained from pyrolysis at 450, 550, and 650 °C.

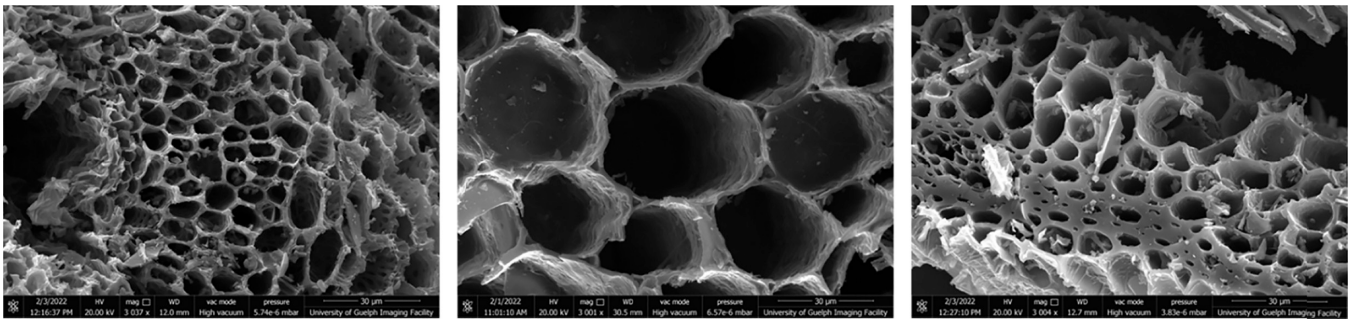

Figure 19. SEM images of switchgrass biocarbon obtained from pyrolysis at 450, 550, and 650 °C.

started losing volatile at 280 °C until 540 °C and experienced a maximum degradation rate at 435 °C. Similarly, S550 lost volatile matters in the temperature range of approx. 280 to 570 °C with maximum degradation at 490 °C. In switchgrass biocarbon, S650 was the most thermally stable sample showing a volatile loss between 280 and 595 °C with a maximum value of 535 °C. The residuals in the samples were decomposed at above 620 °C.

The highest HRI value of the S650 compared to S450 and S550 and H650 compared to H450 and H550 indicates the higher thermal stability of the biocarbon obtained at higher pyrolysis temperatures. The DTG curve further supports the improved thermal stability of the biocarbon obtained at higher pyrolysis temperatures in both feedstocks (hemp stalk and switchgrass).

3.4. Differential Scanning Calorimetry of the Hemp Fiber-Reinforced Composite Samples. The enthalpy

https://doi.org/10.1021/acsomega.3c00700
ACS Omega 2023, 8, 15422−15440

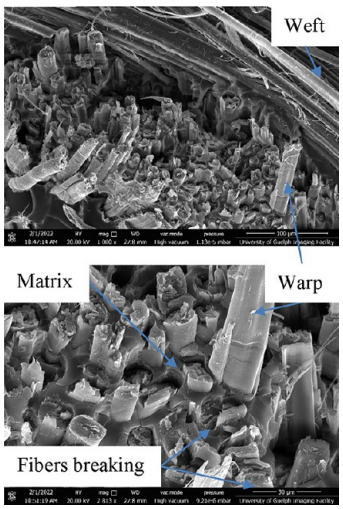

Figure 20. SEM images of hemp fiber-reinforced bioepoxy composites (magnification: 100 μm above and 30 μm below).

changes during the transition between the sample and the surrounding results in DSC thermograms. The DSC experiment determined the glass transition temperature (T_g) at the maximum of the endothermic peak from the second heating scan.[24] The results are shown in Table 3 below.

The glass transition temperature (T_g) helps study the epoxy composites' curing behavior and thermal properties. Table 3 shows the polymer's glass transition temperature in the various composite samples during the DSC analysis. The glass transition point during the first heating cycle increased in the second heating cycle of the hemp biocarbon-filled composite samples. This increase is because the exothermal curing residuals in the second heating cycle get removed and confirm a complete polymerization and polymer chains cross-linking of the resin in the composite samples. Nevertheless, results showed an increase in the glass transition temperature in the second heat cycle; the filler did not significantly affect the glass transition temperature of the composite samples. The average glass transition temperatures of the composites were 76.13 and 76.50 °C for the hemp biocarbon-filled and switchgrass biocarbon-filled hemp fiber-reinforced polymer composites.

3.5. Thermal Conductivity of the Composite Samples.

The thermal conductivity of the studied sustainable composite material ranges between 0.36 and 0.63 $W{\cdot}m^{-1}{\cdot}K^{-1}$, showing their medium to low thermal insulation properties. This range includes the thermal conductivity of epoxy doped with 7.2 wt % copper nanowires and thermally annealed graphene aerogel (0.51 $W{\cdot}m^{-1}{\cdot}K^{-1}$).[46] These materials can potentially be used in construction to insulate walls, roofs, and floors due to their high thermal insulation properties; in the automotive and aerospace industries to make lightweight parts leading to improve fuel efficiency that requires high thermal insulation properties; in creating lightweight and thermally insulated packaging materials; and in the manufacture of furniture, toys, and electronics. Experimental results showed a value of 0.358 (±) $W{\cdot}m^{-1}{\cdot}K^{-1}$ for the thermal conductivity of bioepoxy composite samples without incorporating the fibers and fillers. This value was reduced by 27% to 0.261 $W{\cdot}m^{-1}{\cdot}K^{-1}$ when the hemp fiber was used to reinforce the polymer composite. The insulating thermal property of the hemp fibers is the reason for this enhanced thermal insulating behavior of the resulting composite materials reinforced with hemp. A further result showed that adding biocarbon to the hemp-reinforced composites increased the thermal conductivity of the composite samples. The findings are presented in Table 4 below:

The findings are reported in Figure 7 below. In the biocarbon-filled hemp-reinforced composite sample, the material's conductivity increased by 10 and 17% by increasing the filler content from hemp and switchgrass by 100% from 10 to 20 wt % regardless of the pyrolysis temperature. This result agrees with similar findings by Giorcelli and Bartoli,[47] in which the authors studied the electrical conductivity of the coffee biochar-filled epoxy resin composites. The pyrolysis temperature from 400 to 600 °C did not show a noticeable increase in conductivity, while the value rose to 5.4×10^{-8} S/m when the filler loading was increased by 100%.[47] The increase in thermal

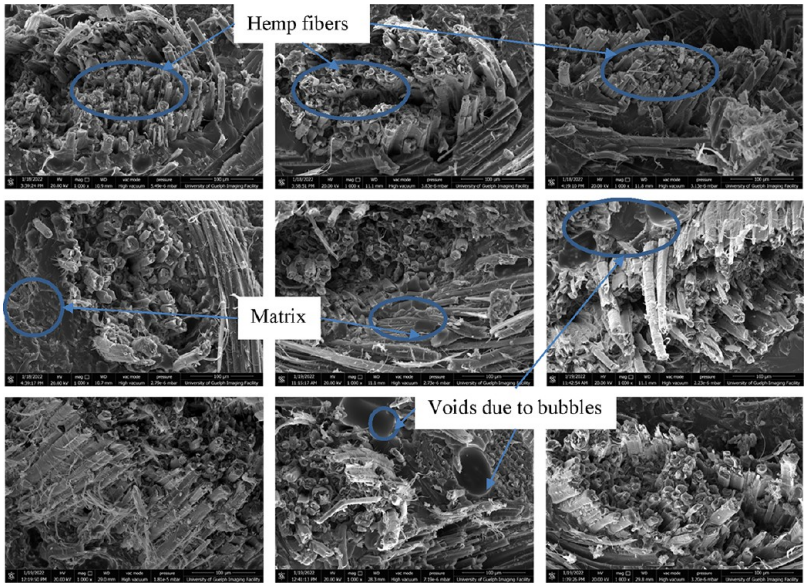

Figure 21. SEM images with magnification 100 μm (from top left in a cyclic order: H45-50-10, H45-50-20, H45-100-10, H65-50-10, H65-100-20, H65-100-10, H65-50-20, H45-100-20, and at the center: H55-75).

https://doi.org/10.1021/acsomega.3c00700
ACS Omega 2023, 8, 15422−15440

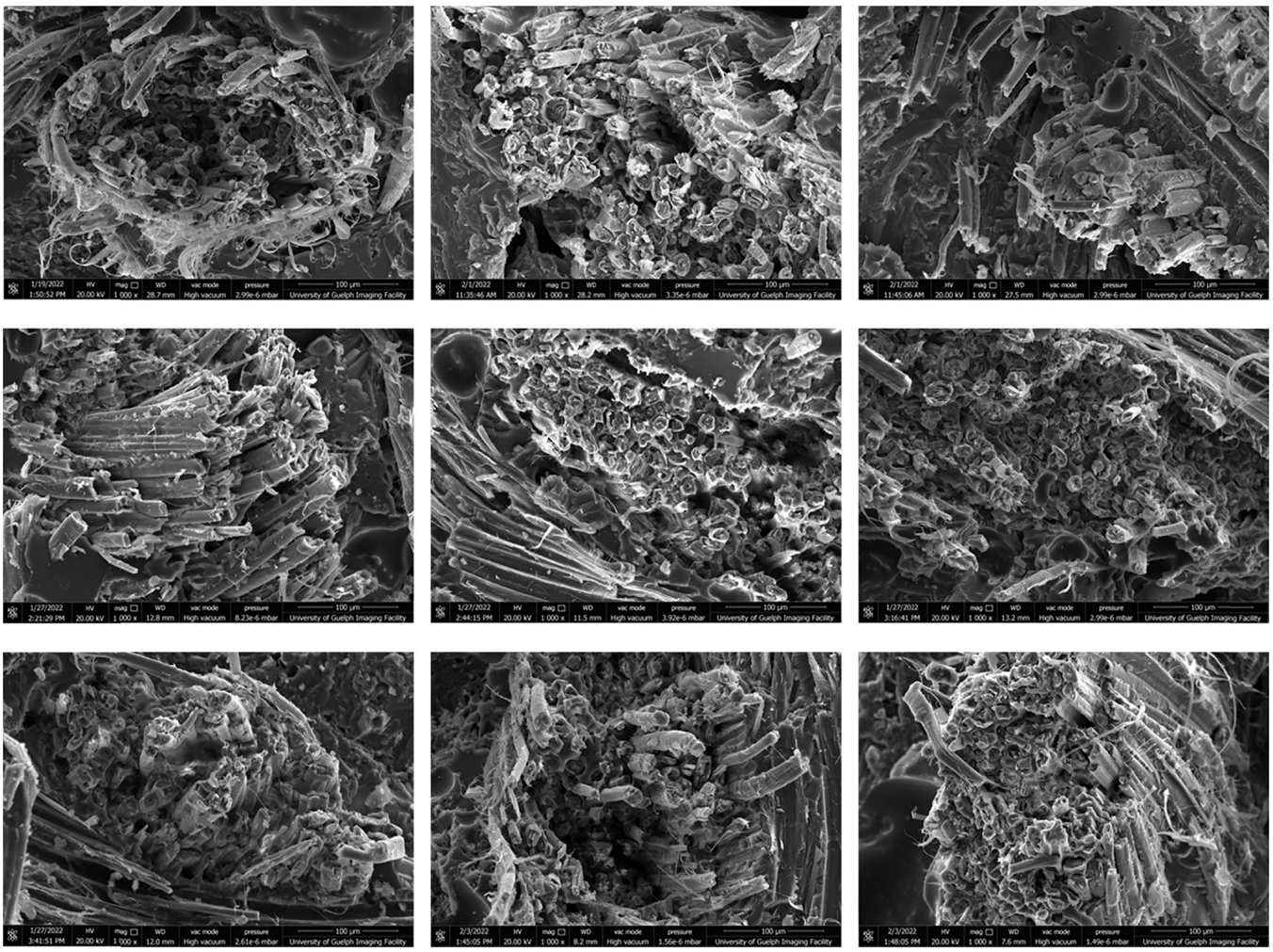

Figure 22. SEM images with magnification of 100 μm (from top left in clockwise: S45-50-10, S45-50-20, S45-100-10, S65-50-10, S65-100-20, S65-100-10, S65-50-20, S45-100-20, and at the center: S55-75).

conductivity with the increased biocarbon filler in the composite was also observed by Adeniyi et al.[48] and Prabhu et al.[49] In addition, the bigger particle size of the filler also positively impacted the thermal conductivity of the composite material. A 50% increase in particle size of the hemp biocarbon biofillers increased the composite samples' mean thermal conductivity by over 10%. The increase in mean thermal conductivity almost tripled when the particle size was doubled from 10 μm. The results were consistent when the switchgrass biocarbon fillers were tested in the composite samples. The study on the impact of the pyrolysis temperature on the thermal conductivity of the hemp-reinforced composite showed an inconclusive result. In hemp biofillers, an increase in pyrolysis temperature from 450 to 550 °C increased the mean thermal conductivity of the samples by 3%, and a further increase in pyrolysis temperature to 650 °C increased the mean thermal conductivity by 10.26% to 0.50 $W \cdot m^{-1} \cdot K^{-1}$. When switchgrass biocarbon was used, the increase in pyrolysis temperature from 450 to 550 °C decreased the mean thermal conductivity of the samples by 5.85%, and the change in mean conductivity value remained almost the same on further raising the temperature to 650 °C.

3.5.1. Statistical Analysis. Results from the ANOVA of the biocarbon-filled hemp-reinforced polymer composites are summarized in Table 5 below.

Removing the insignificant interaction terms in the hemp biocarbon-containing composites, the model *F*-value of 18.10 implies that the model is significant. There is only a 0.01% chance that an *F*-value this large could occur due to noise. The low *p*-values (<0.0500) indicate that model terms are significant. The pyrolysis temperature, particle size, and loading are significant model terms. The lack of fit *F*-value of 0.91 implies that the lack of fit is insignificant relative to the pure error.

Similarly, from the ANOVA of the switchgrass biocarbon results containing composite samples, the model *F*-value of 39.49 implies that the model is significant. There is only a 0.01% chance that an *F*-value this large could occur due to noise. The low *p*-values for A, B, C, AB, BC, and ABC are significant model terms. Moreover, the lack of fit *F*-value of 1.28 implies that the lack of fit is not significant relative to the pure error. The fit statistics summary is presented in Table 6 below:

For the hemp biocarbon-filled biocomposite samples, the predicted R^2 of 0.53 is in reasonable agreement with the adjusted R^2 of 0.59; the difference is less than 0.2. Adequate precision of 12.711 (greater than 4) indicated a sufficient signal that the model could navigate the design space. Similarly, for the switchgrass biocarbon-filled composites samples, the predicted R^2 of 0.8593 is in reasonable agreement with the

https://doi.org/10.1021/acsomega.3c00700
ACS Omega 2023, 8, 15422−15440

adjusted R^2 of 0.9166. Table 7 below offers the coefficients in terms of coded factors.

In Table 7, the coefficient estimate represents the expected change in response per unit change in the factor value when all remaining factors are held constant. The intercept in an orthogonal design is the overall average response of all the runs. The coefficients are adjustments around that average based on the factor settings. When the factors are orthogonal, the VIFs are 1; VIFs greater than 1 indicate multicollinearity.

Furthermore, the coded equations for (i) hemp biocarbon-filled and (ii) switchgrass biocarbon-filled hemp fiber reinforced polymer composites are

$$(\text{thermal conductivity})^{-0.5} = 1.46 - 0.0367 \times A - 0.0795 \times B - 0.0356 \times C \quad (1)$$

$$(\text{thermal conductivity})^{-1.5} = 3.3546 + 0.1980 \times A - 0.5915 \times B - 0.3781 \times C - 0.2160 \times AB - 0.1196 \times BC - 0.1197 \times ABC \quad (2)$$

The high levels and low levels are coded as +1 and − 1, respectively, in the above equations. These eqs 1 and 2 can be used to identify the relative impact of the factors by comparing the factor coefficients of the biocarbon-filled hemp-reinforced polymer composites. Figures 8 and 9 shows the contour plot and the surface response of the thermal conductivity of the hemp biocarbon-filled hemp-reinforced composites.

Similarly, Figures 10 and 11 shows the contour plot and the surface response of the thermal conductivity of the hemp biocarbon-filled hemp-reinforced composites.

3.6. Flame Test. The time to burn the distance of 75 mm on the HaR sample was 128.12 (±2.385) s, and this value increased to 198.73 (±15.368) s when the polymer was reinforced with hemp fiber. Adding hemp and switchgrass biocarbon fillers into the hemp-reinforced composite further changed the flame duration of the composite system. The filler loading positively affected the flame time for both hemp biocarbon and switchgrass-filled biocomposite samples. Similarly, the particle size improved the flame time of the composite material. The burning sample from the flame test is presented as the representative figure in Figure 12.

The result from the flame test is demonstrated in Figure 13 below. It shows a comparison of the flame time of various composite compositions. The flame time has increased with the increase in filler loading and the pyrolysis temperature. The particle size positively influenced the flame time, indicated by the rise in its value when the particle size was increased by 50% to 75 μm and by 100% to 100 μm. Increasing the pyrolysis temperature from 450 to 550 °C reduced the flame time by 3.37 and 8.73%. The flame times were increased by 13.47 and 9.76% for hemp and switchgrass biofillers, respectively, when the temperature was increased to 650 °C. A 50% increase in filler particle size also reduced the flame time by 3 and 7.35%, while the increase in particle size by 100% from 10 to 20 μm improved the sample burning time by 14.49 and 12.93% with hemp and switchgrass fillers, respectively. Also, 50% filler loading negatively affected the fire properties of the composite samples as it showed a decrease of flame time by 1.17 and 5.55% during the process in hemp and switchgrass biocarbon, respectively. Doubling the hemp and switchgrass biocarbon filler loading increased the flame time by 18.32 and 17.07%, respectively. The results showed that the hemp biocarbon fillers are better regarding fire resistance regardless of the pyrolysis temperature, filler size, and loading. The prolonged flame time and increased thermal barrier properties are desirable features in natural fiber-reinforced biocarbon-filled biocomposites for applications where fire resistance and thermal insulation are essential. Natural fiber-reinforced biocarbon-filled biocomposites can be used as insulation materials in buildings, such as for roofs, walls, and floors; in automotive interiors, such as door panels, and dashboards; in the manufacture of interior components of aircraft, such as seats, panels, and cabin partitions, in electrical applications, such as in circuit breakers and switchgear; and in the ship interiors, such as wall panels and ceiling materials, to improve fire resistance and thermal insulation.

3.6.1. Statistical Analysis of the Flame Test. Results from the ANOVA of the biocarbon-filled hemp-reinforced polymer composites are summarized in Table 8 below.

The model F-value of 39.46 (p-value = <0.0001) implies that the model of hemp biocarbon-filled composites model is significant. The lack of fit F-value of 1.06 means that the lack of fit is insignificant relative to the pure error. Similarly, the model F-value of 7.47 (p-value = 0.0014) implies that the model of switchgrass biocarbon-filled biocarbon is significant. The lack of fit F-value of 0.95 means that the lack of fit is insignificant relative to the pure error. The fit statistics for the developed model are presented in Table 9 below:

The statistical model with coded factors for the hemp biocarbon composite samples is shown in eq 3, and the switchgrass biocarbon composite samples are presented in eq 4 below:

$$(\text{flame time})^{2.25} = 2.049 \times 10^5 + 28149.52 \times A + 29619.04 \times B + 38586.33 \times C - 11683.94 \times AB + 9957.35 \times AC + 8562.17 \times BC \quad (3)$$

$$(\text{flame time})^{-1.8} = 0.0001 - 5.115 \times 10^{-6} \times A - 6.156 \times 10^{-6} \times B - 7.313 \times 10^{-6} \times C + 4.226 \times 10^{-6} \times AB \quad (4)$$

The coded factors equations can be used to predict the response for given levels of each element. The high levels of the factors are coded as +1, and the low levels are coded as −1. The coded equations above can be utilized to identify the relative impact of the factors by comparing the factor coefficients. Figures 14 and 15 show the contour plot and the surface response of the flame time of the hemp biocarbon-filled hemp-reinforced composites.

Similarly, Figures 16 and 17 shows the contour plot and the surface response of the flame time of the switchgrass biocarbon-filled hemp-reinforced composites.

3.7. SEM Analysis. Figures 18 and 19 show the SEM images of the biocarbon from hemp and switchgrass feedstock, respectively. The SEM depicts the honeycomb structure of the biocarbon due to the release of the trapped volatile matters in the biomass feedstock. These pores in the biocarbon fillers are filled with the matrix when introduced as the filler material in composite material. The nonconductive void is replaced with polymer with higher thermal conductivity resulting in a rise in the resultant thermal conductivity compared to the individual conductivity of biocarbon or bioepoxy.

https://doi.org/10.1021/acsomega.3c00700
ACS Omega 2023, 8, 15422−15440

The SEM images of the samples after the tension pull are shown in Figures 20−22 below. The photos show the strongly bonded fiber−matrix interfaces in the composite samples. The matrix has neatly wetted the fibers. The thermally insulating hemp fibers have reduced the polymer matrix's thermal conductivity in the composite material. The SEM image can show the orientation and distribution of the hemp fibers in the composite. The figures indicate the even distribution of the fibers along the warp in clusters and bundles. The images also reveal the extent of the interfacial bonding between the hemp fibers and the bioepoxy matrix. The composites have good adhesion between the fiber−matrix interface, while intermittent gaps and voids exist. The smooth penetration of the fiber surface by the matrix shows strong interaction and mechanical interlocking between the hemp fibers and the bioepoxy matrix. The SEM images demonstrate the composite surfaces' morphology, including pits, cracks, and fiber distribution.

4. CONCLUSIONS

This study finds the glass transition temperature of the biocarbon-filled hemp-reinforced polymer composites in the range of 76 °C. The biocarbon filler-filled hemp composites' thermal conductivity was experimentally determined and statistically analyzed. The thermal conductivity of the hemp biocarbon-filled composites was mainly because of biocarbon loading and the filler particle size.

In contrast, the interaction effects of the factors (pyrolysis temperature, particle size, and filler loading) on the thermal conductivity of the switchgrass biocarbon-filled composites were studied. The presence of void, filler, and fiber nature changes the heat transfer behavior through the composite. The filler loading was directly proportional to the thermal conductivity in biocarbon-filled hemp-reinforced polymer composite samples. The effective thermal conductivity increased with increasing grain size. The plant-based bioepoxy composites can have a thermal conductivity range of 0.36 to 0.63 $W{\cdot}m^{-1}{\cdot}K^{-1}$, prolonging the flame time and raising the thermal barrier. These materials with medium to low thermal insulation can be used in building panels, lightweight parts requiring high thermal insulation in automotive and aerospace industries, and lightweight and thermally insulated packaging materials. The determination of thermal conductivities of the hemp fiber-reinforced composite samples is vital to identify and categorize the biobased materials to promote them with their economic importance. The effect of various parameters and constituents is determined with accuracy. These novel composite materials will likely be increasingly important in sustainable manufacturing and construction processes. Using sustainable and renewable materials like hemp and biocarbon aligns with the trend toward eco-friendly and green manufacturing practices.

■ ASSOCIATED CONTENT

Supporting Information

The Supporting Information is available free of charge at https://pubs.acs.org/doi/10.1021/acsomega.3c00700.

Normal plot of the residuals for the thermal conductivity data of the hemp biocarbon-filled hemp-reinforced biopolymer composites; normal plot of the residuals for the thermal conductivity data of the switchgrass biocarbon-filled hemp-reinforced biopolymer composites; normal plot of the residuals for the flame time of the hemp biocarbon-filled hemp-reinforced biopolymer composites; and normal plot of the residuals for the flame time during the fire test of the switchgrass biocarbon-filled hemp-reinforced biopolymer composites (PDF)

■ AUTHOR INFORMATION

Corresponding Authors

Bishnu Acharya − *Department of Chemical and Biological Engineering, University of Saskatchewan, Saskatoon, Saskatchewan S7N 5A9, Canada;* orcid.org/0000-0003-2442-0969; Email: Bishnu.acharya@usask.ca

Animesh Dutta − *School of Engineering, University of Guelph, Guelph, Ontario N1G 2W1, Canada;* orcid.org/0000-0002-9995-807X; Email: adutta@uoguelph.ca

Author

Raj Kumar Dahal − *School of Engineering, University of Guelph, Guelph, Ontario N1G 2W1, Canada*

Complete contact information is available at: https://pubs.acs.org/10.1021/acsomega.3c00700

Author Contributions

Conceptualization, methodology, formal analysis, investigation, writing of the original draft, review, and editing were done by R.K.D.; validation, resource gathering, and supervision were done by B.A. and A.D.; data curation was done by R.K.D. and B.A; project administration and funding acquisition were done by A.D.; software was done by R.K.D., B.A., and A.D. All authors have read and agreed to the final version of the manuscript.

Funding

This work was supported by the Natural Sciences and Engineering Research Council of Canada (NSERC) and Agriculture and Agri-Food Canada's AgriScience program Biomass Canada Cluster.

Notes

The authors declare no competing financial interest.

■ REFERENCES

(1) Pickering, K. L.; Efendy, M. G. A.; Le, T. M. A Review of Recent Developments in Natural Fibre Composites and Their Mechanical Performance. *Composites, Part A* **2016**, *83*, 98−112.

(2) Cao, Y.; Wu, Y. Evaluation of Statistical Strength of Bamboo Fiber and Mechanical Properties of Fiber Reinforced Green Composites. *J. Cent. South Univ. Technol.* **2008**, *15*, 564−567.

(3) Lee, B.-H.; Kim, H.-J.; Yu, W.-R. Fabrication of Long and Discontinuous Natural Fiber Reinforced Polypropylene Biocomposites and Their Mechanical Properties. *Fibers Polym.* **2009**, *10*, 83−90.

(4) Li, X.; Tabil, L. G.; Panigrahi, S. Chemical Treatments of Natural Fiber for Use in Natural Fiber-Reinforced Composites: A Review. *J. Polym. Environ.* **2007**, *15*, 25−33.

(5) Mehta, G.; Mohanty, A. K.; Thayer, K.; Misra, M.; Drzal, L. T. Novel Biocomposites Sheet Molding Compounds for Low Cost Housing Panel Applications. *J. Polym. Environ.* **2005**, *13*, 169−175.

(6) Singha, A. S.; Jyoti, A. Mechanical, Morphological, and Thermal Properties of Chemically Treated Pine Needles Reinforced Thermosetting Composites. *J. Appl. Polym. Sci.* **2013**, *127*, 387−393.

(7) Bao, Q.; He, R.; Liu, Y.; Wang, Q. Multifunctional Boron Nitride Nanosheets Cured Epoxy Resins with Highly Thermal Conductivity and Enhanced Flame Retardancy for Thermal Management Applications. *Composites, Part A* **2023**, *164*, No. 107309.

(8) Zhao, C.; Li, Y.; Liu, Y.; Xie, H.; Yu, W. A Critical Review of the Preparation Strategies of Thermally Conductive and Electrically

Insulating Polymeric Materials and Their Applications in Heat Dissipation of Electronic Devices. *Adv. Compos. Hybrid Mater.* **2023**, *6*, 27.
(9) Shi, X.; Zhang, R.; Ruan, K.; Ma, T.; Guo, Y.; Gu, J. Improvement of Thermal Conductivities and Simulation Model for Glass Fabrics Reinforced Epoxy Laminated Composites via Introducing Hetero-Structured BNN-30@BNNS Fillers. *J. Mater. Sci. Technol.* **2021**, *82*, 239−249.
(10) *Porous Materials*; Elsevier, 2014. DOI: 10.1016/C2012-0-03669-1.
(11) Zhu, D.; Yu, W.; Du, H.; Chen, L.; Li, Y.; Xie, H. Thermal Conductivity of Composite Materials Containing Copper Nanowires. *J. Nanomater.* **2016**, *2016*, 1−6.
(12) KINGERY, W. D. Thermal Conductivity: XII, Temperature Dependence of Conductivity for Single-Phase Ceramics. *J. Am. Ceram. Soc.* **1955**, *38*, 251−255.
(13) Tavman, I. H. Effective Thermal Conductivity of Granular Porous Materials. *Int. Commun. Heat Mass Transfer* **1996**, *23*, 169−176.
(14) Salgado-Delgado, R.; Olarte-Paredes, A.; Salgado-Delgado, A. M.; Vargas-Galarza, Z.; Lopez-Lara, T.; Hernández-Zaragoza, J. B.; Rico-Rodríguez, I.; Martínez-Barrera, G. An Analysis of the Thermal Conductivity of Composite Materials (CPC-30R/Charcoal from Sugarcane Bagasse) Using the Hot Insulated Plate Technique. *Adv. Mater. Sci. Eng.* **2016**, *2016*, 1−5.
(15) Bourai, K.; Riedl, B.; Rodrigue, D. Effect of Temperature on the Thermal Conductivity of Wood-Plastic Composites. *Polym. Polym. Compos.* **2013**, *21*, 413−422.
(16) Nováková, P. Use of Technical Hemp in the Construction Industry. *MATEC Web Conf.* **2018**, *146*, No. 03011.
(17) Allin, S. *Building with Hemp, 2nd Revise.*; SEED PRESS, 2012.
(18) Freivalde, L.; Kukle, S.; Russell, S. Thermal Properties of Hemp Fibre Non-Woven Materials. *IOP Conf. Ser.: Mater. Sci. Eng.* **2013**, *49*, No. 012030.
(19) Park, Y. S.; Joo, C. W. Effects of Nanoparticles on Tensile, Electrical, and Thermal Properties of Hemp/PBTG Composites. *Fibers Polym.* **2016**, *17*, 1934−1944.
(20) Sair, S.; Oushabi, A.; Kammouni, A.; Tanane, O.; Abboud, Y.; El Bouari, A. Mechanical and Thermal Conductivity Properties of Hemp Fiber Reinforced Polyurethane Composites. *Case Stud. Constr. Mater.* **2018**, *8*, 203−212.
(21) Stevulova, N.; Cigasova, J.; Estokova, A.; Terpakova, E.; Geffert, A.; Kacik, F.; Singovszka, E.; Holub, M. Properties Characterization of Chemically Modified Hemp Hurds. *Materials* **2014**, *7*, 8131−8150.
(22) Gümüşkaya, E.; Usta, M.; Balaban, M. Carbohydrate Components and Crystalline Structure of Organosolv Hemp (Cannabis Sativa L.) Bast Fibers Pulp. *Bioresour. Technol.* **2007**, *98*, 491−497.
(23) Tziamtzi, C. K.; Chrissafis, K. Optimization of a Commercial Epoxy Curing Cycle via DSC Data Kinetics Modelling and TTT Plot Construction. *Polymer (Guildf)* **2021**, *230*, No. 124091.
(24) Moriana, R.; Vilaplana, F.; Karlsson, S.; Ribes-Greus, A. Improved Thermo-Mechanical Properties by the Addition of Natural Fibres in Starch-Based Sustainable Biocomposites. *Composites, Part A* **2011**, *42*, 30−40.
(25) Liu, E.; Das, L.; Zhao, B.; Crocker, M.; Shi, J. Impact of Dilute Sulfuric Acid, Ammonium Hydroxide, and Ionic Liquid Pretreatments on the Fractionation and Characterization of Engineered Switchgrass. *Bioenergy Res.* **2017**, *10*, 1079−1093.
(26) Dai, D.; Fan, M. Characteristic and Performance of Elementary Hemp Fibre. *Mater. Sci. Appl.* **2010**, *01*, 336−342.
(27) Kubo, S.; Kadla, J. F. Hydrogen Bonding in Lignin: A Fourier Transform Infrared Model Compound Study. *Biomacromolecules* **2005**, *6*, 2815−2821.
(28) Sills, D. L.; Gossett, J. M. Using FTIR to Predict Saccharification from Enzymatic Hydrolysis of Alkali-Pretreated Biomasses. *Biotechnol. Bioeng.* **2012**, *109*, 353−362.
(29) Asakawa, Y.; Ludwiczuk, A.; Nagashima, F. Phytochemical and Biological Studies of Bryophytes. *Phytochemistry* **2013**, *91*, 52−80.
(30) Cao, Z.; Wang, Z.; Shang, Z.; Zhao, J. Classification and Identification of Rhodobryum Roseum Limpr. and Its Adulterants Based on Fourier-Transform Infrared Spectroscopy (FTIR) and Chemometrics. *PLoS One* **2017**, *12*, No. e0172359.
(31) Janu, R.; Mrlik, V.; Ribitsch, D.; Hofman, J.; Sedláček, P.; Bielská, L.; Soja, G. Biochar Surface Functional Groups as Affected by Biomass Feedstock, Biochar Composition and Pyrolysis Temperature. *Carbon Resour. Convers.* **2021**, *4*, 36−46.
(32) Ramirez, F. J.; Luque, P.; Heredia, A.; Bukovac, M. J. Fourier Transform IR Study of Enzymatically Isolated Tomato Fruit Cuticular Membrane. *Biopolymers* **1992**, *32*, 1425−1429.
(33) Zhuang, J.; Li, M.; Pu, Y.; Ragauskas, A.; Yoo, C. Observation of Potential Contaminants in Processed Biomass Using Fourier Transform Infrared Spectroscopy. *Appl. Sci.* **2020**, *10*, 4345.
(34) Hossain, M. K.; Strezov, V.; Chan, K. Y.; Ziolkowski, A.; Nelson, P. F. Influence of Pyrolysis Temperature on Production and Nutrient Properties of Wastewater Sludge Biochar. *J. Environ. Manage.* **2011**, *92*, 223−228.
(35) Chen, Y.; Yang, H.; Wang, X.; Zhang, S.; Chen, H. Biomass-Based Pyrolytic Polygeneration System on Cotton Stalk Pyrolysis: Influence of Temperature. *Bioresour. Technol.* **2012**, *107*, 411−418.
(36) Chen, B.; Chen, Z.; Lv, S. A Novel Magnetic Biochar Efficiently Sorbs Organic Pollutants and Phosphate. *Bioresour. Technol.* **2011**, *102*, 716−723.
(37) Zolfi Bavariani, M.; Ronaghi, A.; Ghasemi, R. Influence of Pyrolysis Temperatures on FTIR Analysis, Nutrient Bioavailability, and Agricultural Use of Poultry Manure Biochars. *Commun. Soil Sci. Plant Anal.* **2019**, *50*, 402−411.
(38) Ouajai, S.; Shanks, R. A. Composition, Structure and Thermal Degradation of Hemp Cellulose after Chemical Treatments. *Polym. Degrad. Stab.* **2005**, *89*, 327−335.
(39) Himmelsbach, D. S.; Khalili, S.; Akin, D. E. The Use of FT-IR Microspectroscopic Mapping to Study the Effects of Enzymatic Retting of Flax (Linum Usitatissimum L) Stems. *J. Sci. Food Agric.* **2002**, *82*, 685−696.
(40) Lin, D.; Pan, B.; Zhu, L.; Xing, B. Characterization and Phenanthrene Sorption of Tea Leaf Powders. *J. Agric. Food Chem.* **2007**, *55*, 5718−5724.
(41) Nair, R. R.; Mondal, M. M.; Weichgrebe, D. Biochar from Co-Pyrolysis of Urban Organic Wastes—Investigation of Carbon Sink Potential Using ATR-FTIR and TGA. *Biomass Convers. Biorefin.* **2022**, *12*, 4729−4743.
(42) Zimniewska, M. Hemp Fibre Properties and Processing Target Textile: A Review. *Materials* **2022**, *15*, 1901.
(43) Oginni, O.; Singh, K.; Zondlo, J. W. Pyrolysis of Dedicated Bioenergy Crops Grown on Reclaimed Mine Land in West Virginia. *J. Anal. Appl. Pyrolysis* **2017**, *123*, 319−329.
(44) Chiu, Y.-C.; Chou, I.-C.; Tseng, W.-C.; Ma, C.-C. M. Preparation and Thermal Properties of Diglycidylether Sulfone Epoxy. *Polym. Degrad. Stab.* **2008**, *93*, 668−676.
(45) Hafiezal, M. R. M.; Khalina, A.; Zurina, Z. A.; Azaman, M. D. M.; Hanafee, Z. M. Thermal and Flammability Characteristics of Blended Jatropha Bio-Epoxy as Matrix in Carbon Fiber−Reinforced Polymer. *J. Compos. Sci.* **2019**, *3*, 6.
(46) Yang, X.; Fan, S.; Li, Y.; Guo, Y.; Li, Y.; Ruan, K.; Zhang, S.; Zhang, J.; Kong, J.; Gu, J. Synchronously Improved Electromagnetic Interference Shielding and Thermal Conductivity for Epoxy Nanocomposites by Constructing 3D Copper Nanowires/Thermally Annealed Graphene Aerogel Framework. *Composites, Part A* **2020**, *128*, No. 105670.
(47) Giorcelli, M.; Bartoli, M. Development of Coffee Biochar Filler for the Production of Electrical Conductive Reinforced Plastic. *Polymers (Basel)* **2019**, *11*, 1916.
(48) Adeniyi, A. G.; Abdulkareem, S. A.; Ighalo, J. O.; Onifade, D. V.; Adeoye, S. A.; Sampson, A. E. Morphological and Thermal Properties of Polystyrene Composite Reinforced with Biochar from

https://doi.org/10.1021/acsomega.3c00700
ACS Omega 2023, 8, 15422−15440

Elephant Grass (Pennisetum Purpureum). *J. Thermoplast. Compos. Mater.* **2022**, *35*, 1532−1547.
(49) Prabhu, P.; Jayabalakrishnan, D.; Balaji, V.; Bhaskar, K.; Maridurai, T.; Prakash, V. R. A. Mechanical, Tribology, Dielectric, Thermal Conductivity, and Water Absorption Behaviour of Caryota Urens Woven Fibre-Reinforced Coconut Husk Biochar Toughened Wood-Plastic Composite. *Biomass Convers. Biorefin.* **2022**, 1−8.

https://doi.org/10.1021/acsomega.3c00700
ACS Omega 2023, 8, 15422−15440